On the solution of a 'solvable' model of an ideal glass of hard spheres displaying a jamming transition

On the solution of a 'solvable' model of an ideal glass of hard spheres displaying a jamming transition

Marc Mézard[1,5], **Giorgio Parisi**[2,6], **Marco Tarzia**[3,7] **and Francesco Zamponi**[4,8]

[1] Laboratoire de Physique Théorique et Modèles Statistiques, Batiment 100, Université Paris Sud and CNRS, F-91405 Orsay, France
[2] Dipartimento di Fisica, Sapienza Universitá di Roma, INFN, Sezione di Roma I, IPFC—CNR, Piazzale Aldo Moro 2, I-00185 Roma, Italy
[3] Laboratoire de Physique Théorique de la Matière Condensée, Université Pierre et Marie Curie—Paris 6, UMR CNRS 7600, 4 place Jussieu, F-75252 Paris Cedex 05, France
[4] Laboratoire de Physique Théorique, École Normale Supérieure, UMR CNRS 8549, 24 Rue Lhomond, F-75231 Paris Cedex 05, France

Abstract. We discuss the analytical solution through the cavity method of a mean-field model that displays at the same time an ideal glass transition and a set of jamming points. We establish the equations describing this system, and we discuss some approximate analytical solutions and a numerical strategy to solve them exactly. We compare these methods and we get insight into the reliability of the theory for the description of finite dimensional hard spheres.

Keywords: classical phase transitions (theory), phase diagrams (theory), cavity and replica method, structural glasses (theory)

[5] http://lptms.u-psud.fr/membres/mezard/

[6] http://chimera.roma1.infn.it/GIORGIO/

[7] E-mail: marco.tarzia@lptmc.jussieu.fr

[8] http://www.lpt.ens.fr/~zamponi

*J. Stat. Mech.* (2011) P03002

Contents

1. Introduction

The theoretical investigation of the glass transition and its relation to jamming in hard sphere systems has made considerable progress in the last 30 years [1]–[5]. This has been possible mainly because of the powerful analogy between jammed states and inherent structures [3], [6]–[8] and of the development of methods based on spin glass theory [9, 10] to describe the glass transition of particle systems. This progress led to the proposal that amorphous jammed states of hard spheres can be thought of as the states obtained in the infinite pressure limit of metastable glasses, and therefore described using tools of (metastable-)equilibrium statistical mechanics.

The phase diagram of hard spheres that results from these mean-field studies is summarized in figure 1, where we plot the pressure as a function of the packing fraction φ, which is the fraction of space covered by the spheres. The full black line represents the equilibrium phase diagram with the liquid-to-crystal transition. If this transition can be avoided (by compressing fast enough or by introducing some degree of polydispersity), one enters into a metastable liquid phase. The nature of this metastable liquid changes at $\varphi = \varphi_{\mathrm{d}}$. It consists of a single ergodic state for $\varphi < \varphi_{\mathrm{d}}$. When $\varphi > \varphi_{\mathrm{d}}$, the available phase space splits into many glassy states. If the system is stuck in one of these states and compressed, it follows one of the glass branches of the phase diagram, until its pressure eventually diverges at some packing fraction φ_j which depends on the state. At density φ_{K} a thermodynamic glass transition happens (in the sense of mean-field spin glasses [11]) towards an ideal glass. The pressure of the latter diverges at φ_{GCP}. In the inset, the complexity, i.e. the logarithm of the number of glassy states, is plotted as a function of the jamming density φ_j; this approach predicts that there exist jammed states in a finite interval of density $\varphi_j \in [\varphi_{\mathrm{th}}, \varphi_{\mathrm{K}}]$. The boxes show a schematic picture of the ($3N$-dimensional, where N is the number of particles) phase space of the system: black configurations are allowed by the hard-core constraint, white ones are forbidden. In the supercooled liquid phase the allowed configurations form a connected domain; however, on approaching φ_{d} the connections between different metastable regions become smaller and smaller. Above φ_{K}, they disappear in the thermodynamic limit and glassy states are well defined.

The above mean-field picture has been obtained by a succession of works which started from the studies of some categories of spin glasses with so-called 'one-step replica symmetry breaking', and have gradually matured into analytic approximation tools for the theory of hard spheres (see [5] and references therein). A very interesting model has been introduced recently by Mari *et al* [12]. It displays exactly the phase diagram presented in figure 1: it undergoes an equilibrium glass transition and it has an interval of densities where it shows all the phenomenology which is now associated with jamming, like marginal mechanical stability and the associated presence of anomalous soft modes in the vibrational spectrum [13]–[15]. The model has been studied numerically in [12] in order to show the existence of separate glass and jamming transitions and to clarify to some extent the relation between the two.

This model is interesting in that it is in principle solvable: it can be investigated by means of modern methods that have been developed in the context of mean-field spin glasses, the replica method [16] and the cavity method [17]. This investigation is the purpose of the present paper, where we derive the cavity equations that describe the
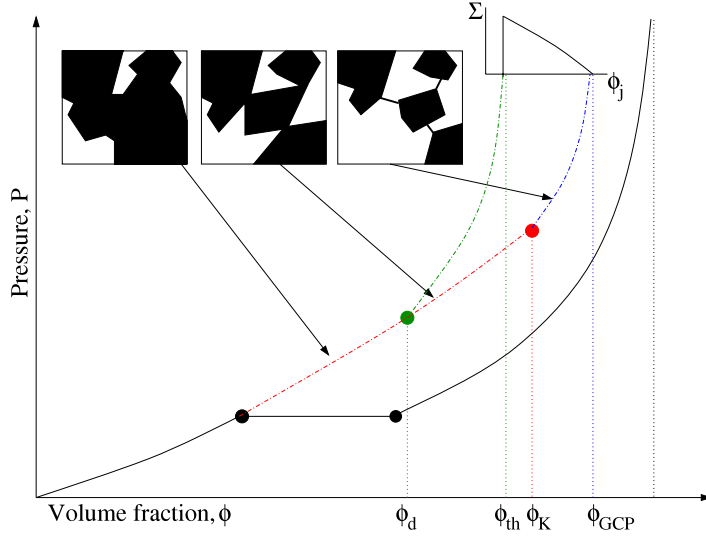
Figure 1. Schematic mean-field phase diagram of hard spheres in three dimensions; see the text and [5] for a detailed description.

model and we present some approximated analytical solutions to them, along with a detailed numerical resolution. Since it will turn out that the exact solution requires quite heavy numerical calculations (heavier than a direct Monte Carlo study of the model, at least for a moderate number of particles, such as the one performed in [12]), one might wonder why this solution is interesting at all. There are at least two reasons why this study is interesting, in our opinion. The first is that Monte Carlo methods are not able to access the deep glassy phase or the densest part of the jammed phase: they are confined to exploration of the region close to $\varphi_{\rm d}$ (at equilibrium) and $\varphi_{\rm th}$ (at jamming). Therefore if one wants to study, for instance, how the properties of the packings change when going from $\varphi_{\rm th}$ to $\varphi_{\rm GCP}$, the exact solution is needed. Moreover, we will show that the cavity method allows us to derive simple analytical approximations to the true solution. Similar approximations have been used to study finite dimensional hard spheres [5]; their investigation in the controlled setting of the present 'solvable' model allows us to assess their reliability. Finally, there are some generic structures in the correlations of jammed packings that researchers would like to explain analytically. Our work is a first step in this direction.

This paper is meant to be read by specialists in the field, so we did not make much attempt to explain in details the basis of the method. Recent complete reviews of the physical problem [5], [18]–[20] as well as of the method we used [17, 21] exist, and the reader is assumed to be familiar with these concepts.

2. Definitions

The model that we study in this paper is a simple generalization of the one introduced in [12], defined as follows. We consider a 'factor graph', namely a bipartite graph made by two types of nodes: variables and boxes. Each variable is connected to z boxes and each box is connected to p variables. In a system with N variables the number of boxes is Nz/p

4
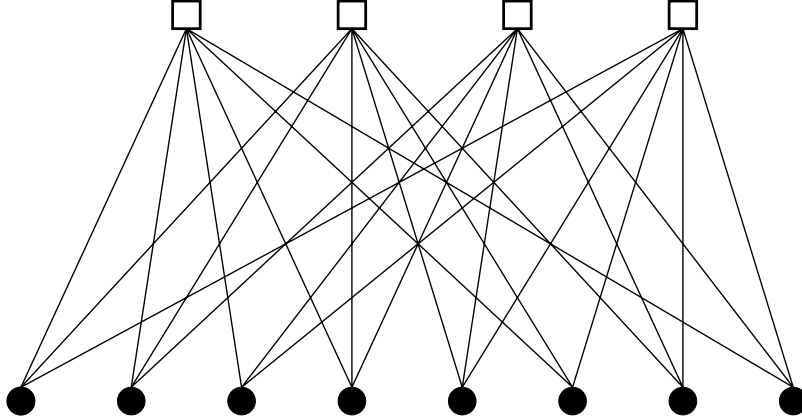
Figure 2. An illustration of the model for $p = 6$, $z = 3$ and $N = 8$. Each white square is a box, each black dot is a variable (sphere). Each box contains all the spheres connected to it by a link. The spheres inside one box must not overlap (note that for $z = 1$ one obtains N/p systems of p hard spheres).

and the total number of links (i.e. variable–box connections) is Nz. We will consider an ensemble of 'random regular' factor graphs where each graph satisfying this requirement has the same probability. A crucial property of this ensemble, that allows for the solution of the model, is that in the thermodynamic limit $N \to \infty$ almost all graphs are locally tree-like, in a sense that can be defined precisely [17].

Each variable is a vector $x_i \in [0,1]^d$ with periodic boundary conditions, where d is the dimension and $i = 1, \ldots, N$. In the following we denote by $|x_i - x_j| = \sqrt{\sum_{\mu=1}^{d}(|x_i^\mu - x_j^\mu|_{\mathrm{mod}1})^2}$ the distance between x_i and its closest periodic image of x_j. If we call $\chi(x_i, x_j)$ the characteristic function of the hard sphere constraint (with periodic boundary conditions), i.e. $\chi(x_i, x_j) = 1$ if $|x_i - x_j| \geq D$ and 0 otherwise, then each box $a = 1, \ldots, Nz/p$ imposes the condition

$$\chi(a) \equiv \chi(x_1^a, \ldots, x_p^a) \equiv \prod_{i<j}^{1,p} \chi(x_i^a, x_j^a) \neq 0, \tag{1}$$

where x_i^a are the variables connected to box a. The partition function of the model is

$$Z = \int \mathrm{d}x_1 \cdots \mathrm{d}x_N \prod_{a=1}^{Nz/p} \chi(a). \tag{2}$$

A pictorial description of the model is the following (see figure 2). Each box can be thought of as a cubic region $[0,1]^d$ with periodic boundary conditions. Each variable node $i = 1, \ldots, N$ represents a 'sphere' of diameter D and this sphere appears in position x_i in all the z boxes to which the node is connected. On the other hand, each box contains exactly p spheres. The constraint is that, for each box, the p spheres present in the box do not overlap.

The model therefore differs from a standard hard sphere model, since each sphere interacts only with a finite subset of neighbors, and the topology of the interaction network

is fixed by the random graph construction described above. This structure is such that the model becomes a mean-field model and is therefore exactly solvable, at least in principle, as we will discuss in the following. It is worth noting, however, that there are two 'formal' limits where one gets back the standard hard sphere model: in the case $z = 1$ the model reduces to N/p independent systems of p hard spheres each, while for $p = 2$ and $z = N - 1$ one gets back a single system of N hard spheres. Note also that in [12] only the version with $p = 2$ has been studied.

Our investigations showed, however, that the model defined above undergoes a 'crystallization' phenomenon at high density: the spheres tend to localize around a discrete set of positions inside the unit box. This has been avoided in [12] by introducing a small degree of polydispersity of the size of the spheres. Here, in the analytical treatment of the model, we do not need to use this trick since we can impose directly that the solutions are translationally invariant, therefore discarding all crystalline phases of the model. In this way one effectively restricts to the amorphous phases, but one should keep in mind that these are metastable with respect to the crystal in the true model. Another possibility to remove the non-translationally invariant phase is to introduce local 'random shifts': on each link we introduce a quenched variable $s_{ai} \in [0, 1]^d$, such that the corresponding particle appears in the corresponding box translated by s_{ai}. On a tree with open boundary conditions, this will not change the model since one can always perform a change of variable to remove the shifts. In the presence of loops however, the random shifts will frustrate the periodic order. But since the cavity solution is based on local recursions, the solutions describing the model with random shifts will be the same as the translationally invariant solutions of the model without random shifts. A similar situation occurs when studying an antiferromagnetic model on a random graph: local recursion relations allow both an antiferromagnetic and an amorphous ordering. The former is irrelevant on a random graph because long loops of odd length frustrate the antiferromagnetic order. The antiferromagnetic system thus behaves like the spin glass in which the signs of the couplings are quenched random variables. See [25] for a more detailed discussion in the context of a very similar model.

We define $V_d(R)$ as the volume of a d-dimensional hypersphere of radius R; then $V_s = V_d(D/2) = 2^{-d}V_d(D)$ is the volume of one hard sphere (since the spheres have diameter D), and $\varphi = pV_s$ is the packing fraction, that represents the fraction of the unit box that is covered by the p interacting spheres. It is trivial to check that there are no configurations with $\varphi > 1$. The parameter that controls the packing fraction is the diameter D since the box size is fixed; for this reason in the following we will use directly the sphere diameter D as control parameter and label the different transitions as D_{K}, D_{GCP}, D_{d}, etc.

For a system of p hard spheres in d dimensions, we define the following quantities:

$$Z_p^0 = \int \mathrm{d}x_1 \cdots \mathrm{d}x_p \prod_{i<j}^{1,p} \chi(x_i, x_j),$$

$$g_p^0(x - y) = \frac{1}{p(p-1)} \left\langle \sum_{i \neq j}^{1,p} \delta(x - x_i)\delta(y - x_j) \right\rangle = \frac{1}{Z_p^0} \int \mathrm{d}x_3 \cdots \mathrm{d}x_p \chi(x, y, x_3, \ldots, x_p),$$

(3)

6

such that Z_p^0 is the partition function of p hard spheres (apart from a $p!$), and g_p^0 is related to the usual pair correlation function [22] by

$$g(r) = \frac{p-1}{p} g_p^0(r).$$

(4)

For the following discussion, it will be useful to define

$$v_n(x_1, \dots, x_n) = \int \mathrm{d}x \prod_{i=1}^{n} \chi(x, x_i),$$

(5)

which is the so-called *void space* or *cavity volume*, namely the volume available to insert an additional sphere in a box given the positions of n other spheres, $\{x_1, \dots, x_n\}$.

3. Cavity equations

The cavity method has now become a standard method to solve statistical models defined on random graphs. We will not explain the method here and refer the reader to [17, 23]. Here we only write the equations for our specific case.

3.1. Bethe free energy

We define by ∂i the set of boxes connected to variable i, and by ∂a the set of variables connected to box a. On each link we define two fields: $\varphi_{a \to i}(x_i)$ is the probability density of the variable x_i when connected only to the box a; $\psi_{i \to a}(x_i)$ is the probability density of the same variable when connected to all the boxes in its neighborhood except a. Both are normalized to one and they satisfy the equations

$$\psi_{i \to a}(x_i) = \frac{1}{Z_{i \to a}} \prod_{b \in \partial i \backslash a} \varphi_{b \to i}(x_i), \qquad \varphi_{a \to i}(x_i) = \frac{1}{Z_{a \to i}} \int \left(\prod_{j \in \partial a \backslash i} \mathrm{d}x_j \, \psi_{j \to a}(x_j) \right) \chi(a), \quad (6)$$

which can derived from the stationarity of the Bethe entropy

$$S = - \sum_{\text{links } a-i} \log \int \mathrm{d}x_i \, \psi_{i \to a}(x_i) \varphi_{a \to i}(x_i) + \sum_a \log \int \left(\prod_{j \in \partial a} \mathrm{d}x_j \, \psi_{j \to a}(x_j) \right) \chi(a)$$
$$+ \sum_i \log \int \mathrm{d}x_i \prod_{a \in \partial i} \varphi_{a \to i}(x_i).$$

(7)

These equations have the general form of the cavity (or Bethe) equations that can be derived for any model with local interactions [17]. With respect to previous studies of frustrated systems with the cavity method, the main difference here (and the main source of difficulty) is the fact that the variables x are *continuous*. Although the Bethe free energy is not variational in general, it has the property that the cavity equations can be obtained imposing its stationarity with respect to the cavity fields. In some special cases one can argue that it provides indeed an upper or lower bound to the true free energy, but a proof of this is still lacking.

3.2. Replica symmetric cavity equations

The replica symmetric (RS) equations for such a regular graph are trivially obtained by dropping the spatial dependence of the fields. In this case we use the notation $Z_\varphi = Z_{a\to i}$ and $Z_\psi = Z_{i\to a}$, and we get

$$\psi(x) = \frac{1}{Z_\psi^{\text{RS}}} \varphi(x)^{z-1}, \qquad \varphi(x) = \frac{1}{Z_\varphi^{\text{RS}}} \int \left(\prod_{j=1}^{p-1} \mathrm{d}x_j\, \psi(x_j) \right) \chi(x, x_1, \ldots, x_{p-1}), \tag{8}$$

and the RS entropy per particle is

$$S_{\text{RS}} = -z \log \int \mathrm{d}x\, \psi(x)\varphi(x) + \frac{z}{p} \log \int \left(\prod_{j=1}^{p} \mathrm{d}x_j\, \psi(x_j) \right) \chi(x_1, \ldots, x_p) + \log \int \mathrm{d}x\, \varphi(x)^z. \tag{9}$$

These equations admit the trivial translationally invariant solution $\psi(x) = \varphi(x) = 1$ with $Z_\psi^{\text{RS}} = 1$ and

$$Z_\varphi^{\text{RS}} = \int \mathrm{d}x \int \left(\prod_{j=1}^{p-1} \mathrm{d}x_j\, \psi(x_j) \right) \chi(x, x_1, \ldots, x_{p-1}) \equiv Z_p^0; \tag{10}$$

that is the partition function of p hard spheres in the unit box. Therefore the entropy of the RS phase is

$$S_{\text{RS}} = \frac{z}{p} \log Z_p^0. \tag{11}$$

3.3. One-step replica symmetry breaking cavity equations

In the standard interpretation [17], the glass phase is signaled by the appearance of multiple solutions $\psi_{i\to a}^{(\alpha)}$, $\varphi_{a\to i}^{(\alpha)}$ of equation (6). Each of these solutions represents a glass state with entropy s_α given by the Bethe entropy (7) computed on the corresponding set of fields. Although one does not have direct access to individual glassy solutions (since the direct numerical solution of the Bethe equations by iteration on a single graph is extremely unstable in this region), a statistical treatment of the properties of the solutions in this regime exists and goes under the name of the one-step replica symmetry breaking (1RSB) description [23]. It is based on an entropy $S(m)$ which is the sum over all solutions α of the corresponding partition function $Z_\alpha = \mathrm{e}^{Ns_\alpha}$ to power m [9]. The latter is computed by looking to the evolution of the solutions of the Bethe equations under an iteration that adds one more variable to the graph [23], or more simply by introducing an auxiliary model and assuming that an RS description holds for that model [17]. We do not discuss

here these derivations and only report the resulting equations for our model, which are the following:

$$S(m) = \frac{1}{N} \log \sum_\alpha Z_\alpha^m = ms(m) + \Sigma(m) = -zS_{\text{link}}(m) + \frac{z}{p}S_{\text{box}}(m) + S_{\text{site}}(m),$$

$$S_{\text{link}}(m) = \log \int d\mathcal{P}[\psi] \, d\mathcal{P}[\varphi] \left[\int dx \, \psi(x)\varphi(x) \right]^m \equiv \log\langle Z_{\text{link}}^m \rangle,$$

$$S_{\text{box}}(m) = \log \int d\mathcal{P}[\psi_1] \cdots d\mathcal{P}[\psi_p] \left[\int \left(\prod_{j=1}^p \psi_j(x_j) \, dx_j \right) \chi(x_1, \ldots, x_p) \right]^m \equiv \log\langle Z_{\text{box}}^m \rangle, \quad (12)$$

$$S_{\text{site}}(m) = \log \int d\mathcal{P}[\varphi_1] \cdots d\mathcal{P}[\varphi_z] \left[\int dx \prod_{i=1}^z \varphi_i(x) \right]^m \equiv \log\langle Z_{\text{site}}^m \rangle.$$

The stationarity of this function with respect to $\mathcal{P}[\psi]$ and $\mathcal{P}[\varphi]$ gives the 1RSB equations:

$$\mathcal{P}[\psi] = \frac{1}{\mathcal{Z}_\psi} \int \prod_{i=1}^{z-1} d\mathcal{P}[\varphi_i] \, \delta\left[\psi(x) - \frac{1}{Z_\psi} \prod_i \varphi_i(x) \right] (Z_\psi)^m,$$

$$\mathcal{P}[\varphi] = \frac{1}{\mathcal{Z}_\varphi} \int \prod_{i=1}^{p-1} d\mathcal{P}[\psi_i] \, \delta\left[\varphi(x) - \frac{1}{Z_\varphi} \int \prod_j dx_j \, \psi_j(x_j)\chi(x, x_1, \ldots, x_{p-1}) \right] (Z_\varphi)^m, \quad (13)$$

where the normalization constants are

$$Z_\psi[\varphi_1, \ldots, \varphi_{z-1}] = \int dx \prod_i \varphi_i(x),$$

$$Z_\varphi[\psi_1, \ldots, \psi_{p-1}] = \int dx \prod_j dx_j \, \psi_j(x_j)\chi(x, x_1, \ldots, x_{p-1}), \quad (14)$$

$$\mathcal{Z}_\psi = \langle (Z_\psi)^m \rangle, \qquad \mathcal{Z}_\varphi = \langle (Z_\varphi)^m \rangle.$$

The internal entropy can then be written, using the standard method of [9], as

$$s(m) = \frac{\partial S(m)}{\partial m} = -z\frac{\langle Z_{\text{link}}^m \log Z_{\text{link}} \rangle}{\langle Z_{\text{link}}^m \rangle} + \frac{z}{p}\frac{\langle Z_{\text{box}}^m \log Z_{\text{box}} \rangle}{\langle Z_{\text{box}}^m \rangle} + \frac{\langle Z_{\text{site}}^m \log Z_{\text{site}} \rangle}{\langle Z_{\text{site}}^m \rangle} \quad (15)$$

and the complexity is $\Sigma(m) = S(m) - ms(m)$. The parameter m is the 1RSB parameter, whose equilibrium value must be fixed imposing that the replicated entropy is stationary [16].

4. The stability of the RS solution

To study the stability of the RS phase we perturb around it:

$$\psi_{i \to a}(x) = 1 + A e^{-ikx + i\theta_{i \to a}}, \quad (16)$$

and look at the linear stability of A assuming that the phase θ is random, i.e. when substituting in the right-hand side of (8) each ψ gets a random independent phase. This is done in order to enforce translational invariance; otherwise we would study the instability

towards modulated phases, which is indeed interesting, but we do not consider it here, for reasons discussed in section 1. Note that we have $k = 2\pi(n_1, \ldots, n_d)$, where n_i are integer numbers. Then at first order we have

$$A e^{-ikx+i\theta} = A \frac{1}{Z_p^0} \sum_{a=1}^{z-1} \sum_{j=1}^{p-1} \int dx_2 \cdots dx_p \, \chi(x, x_2, \ldots, x_p) e^{-ikx_2 + i\theta_{j \to a}}. \qquad (17)$$

Now we can bring the factor e^{-ikx} on the other side and integrate over x; moreover we take the square and use that the $\theta_{j \to a}$ are random and uncorrelated and we obtain the final result

$$A^2 = A^2(z-1)(p-1) \left| \frac{1}{Z_p^0} \int dx_1 \cdots dx_p \, \chi(x_1, \ldots, x_{p-1}) e^{ik(x_1-x_2)} \right|^2. \qquad (18)$$

Defining

$$g_p^0(k) = \int dx \, dy \, e^{ik(x-y)} g_p^0(x-y) = \frac{1}{Z_p^0} \int dx_1 \cdots dx_p \, \chi(x_1, \ldots, x_p) e^{ik(x_1-x_2)}, \qquad (19)$$

the stability condition is

$$\sqrt{(p-1)(z-1)} |g_p^0(k)| \leq 1, \qquad \forall k = 2\pi(n_1, \ldots, n_d) \neq 0. \qquad (20)$$

Hence from the knowledge of Z_p^0 and $g_p^0(k)$ we can compute the RS entropy and the stability of the RS solution.

4.1. Results for $p = 2$, any dimension

For $p = 2$, $k \neq 0$ and $D < 1/2$, we have simply $g_2^0(x-y) = \chi(x-y)/(1-V_d(D))$ and

$$g_2^0(k) = \int_{[0,1]^d} dx \, \frac{e^{ikx} \chi(x)}{1-V_d(D)} = -\int_{[-1/2,1/2]^d} dx \, \frac{e^{ikx} \theta(|x| < D)}{1-V_d(D)} = -\left(\frac{2\pi D}{k} \right)^{d/2} \frac{J_{d/2}(kD)}{1-V_d(D)}. \qquad (21)$$

One can show that for the values of D we are interested in, the maximum of $g_2^0(k)$ is assumed for $k = 2\pi$, i.e. the smallest k. Then the condition on D is

$$\frac{D^{d/2} J_{d/2}(2\pi D)}{1-V_d(D)} \leq \frac{1}{\sqrt{z-1}}. \qquad (22)$$

In the limit $z \to \infty$, as D is small, we can use $J_n(x) \sim (x/2)^n/\Gamma(n+1)$, and neglecting the denominator

$$\frac{D^{d/2} J_{d/2}(2\pi D)}{1-V_d(D)} \sim \frac{\pi^{d/2} D^d}{\Gamma(d/2+1)} = V_d(D) \leq \frac{1}{\sqrt{z-1}}. \qquad (23)$$

4.2. Results for $d = 1$, any p

In $d = 1$ we get, from the exact solution,

$$Z_p^0 = [1-pD]^{p-1}, \qquad g_p^0(k) = \frac{1}{p-1} \sum_{n=0}^{p-2} e^{-i(n+1)kD} {}_1F_1[1+n; p; -i(1-pD)k], \qquad (24)$$

where ${}_1F_1[a; b; z]$ is the confluent hypergeometric function of the first kind. Also in this case the lowest k becomes unstable in the first place.

4.3. Results for $d = 2$ and $p = 3$

As a last interesting case, we consider $d = 2$ and $p = 3$. In the following for simplicity we consider $D < 1/4$ to avoid problems coming from periodic boundary conditions.

We start by the computation of the partition function Z_3^0 of three spheres in a box, which can be done using the standard virial expansion. For convenience we fix the first sphere, as well as the origin of the coordinate frame, in the center of the box. The center of the second sphere can be anywhere in the box outside a disc of radius D centered in the origin. Given the position of the second sphere, the third sphere can be anywhere outside the union of two discs centered around the first two spheres.

If the second sphere is at distance $r = |x_2 - x_1|$ from the origin $x_1 = 0$, the free volume accessible to the third sphere is

$$v_2(x_1, x_2) = 1 - 2\pi D^2 + \theta(2D - r)D^2 \left(2\arccos \frac{r}{2D} - \frac{r}{2D}\sqrt{4 - \frac{r^2}{D^2}} \right). \tag{25}$$

This has to be integrated over the position of the second sphere. There are three possible cases.

(1) $r \in [D, 2D]$; in this case the first and second exclusion spheres have an overlap, and the second sphere can rotate at any angle without hitting the boundary of the box. Therefore one has

$$Z_3^0(1) = 2\pi \int_D^{2D} dr\, r \left[1 - 2\pi D^2 + D^2 \left(2\arccos \frac{r}{2D} - \frac{r}{2D}\sqrt{4 - \frac{r^2}{D^2}} \right) \right]. \tag{26}$$

(2) $r \in [2D, 1/2]$ (recall that the box has side 1 so r is at most $1/2$); in this case the first and second exclusion spheres have no overlap, and the second sphere can rotate at any angle, therefore

$$Z_3^0(2) = 2\pi \int_{2D}^{1/2} dr\, r(1 - 2\pi D^2). \tag{27}$$

(3) $r \in [1/2, \sqrt{2}/2]$; also in this case there is no overlap contribution, but the second sphere can only be at some angles because of the cubic shape of the box. The total angle that can be spanned is $8(\pi/4 - \arccos(1/(2r)))$, therefore

$$Z_3^0(3) = 8 \int_{1/2}^{\sqrt{2}/2} dr\, r(1 - 2\pi D^2) \left(\frac{\pi}{4} - \arccos\left(\frac{1}{2r}\right) \right). \tag{28}$$

All the integrals can be evaluated and summing the three contributions one gets the final result

$$Z_3^0 = 1 - 3\pi D^2 + \tfrac{1}{4}\pi D^4(3\sqrt{3} + 8\pi), \qquad D < 1/4. \tag{29}$$

We also need the value of the pair correlation at contact, $g_3^0(D)$. Following the same reasoning this is given by

$$g_3^0(D) = \frac{v_2(r = D)}{Z_3^0} = \frac{1 - 2\pi D^2 + D^2(2\pi/3 - \sqrt{3}/2)}{1 - 3\pi D^2 + 1/4\pi D^4(3\sqrt{3} + 8\pi)}, \qquad D < 1/4. \tag{30}$$

Finally, $g_3^0(x - y) = v_2(x, y)/Z_3^0$, from which one can compute $g_3^0(k)$ numerically and determine the stability of the RS solution.

5. The Gaussian approximation

We now introduce an approximation to describe the 1RSB phase of the model. We assume that the fields $\psi_j(x)$ and $\varphi_i(x)$ are localized around a position which is randomly distributed in the box (this maintains the global translational invariance). This ansatz, of course, is not a solution of the 1RSB equations. However, we expect that it provides a reasonable estimate of $S(m)$, which is expected to become more and more accurate for large connectivity and close to the random close packing point. Moreover, we will see in the following that, even if the variational nature of the replicated entropy cannot be proven, these approximations give upper bounds for D_{K}. For this reason we will refer from now on to these approximations as 'variational' approximations. Note that if a variational approximation predicts that the Kauzmann radius is less than the radius where the RS solution is unstable, $D_{\mathrm{K}} < D_{\mathrm{RS}}$, then we know for sure that there is a discontinuous transition occurring at a value of D smaller than D_{RS}.

We assume a Gaussian shape for the fields, which leads to the following assumption for their distribution:

$$\mathcal{P}[\psi] = \int \mathrm{d}X \, \delta \left[\psi(x) - \frac{\mathrm{e}^{-(x-X)^2/2A}}{(2\pi A)^{d/2}} \right], \qquad \mathcal{P}[\varphi] = \int \mathrm{d}X \, \delta \left[\varphi(x) - \frac{\mathrm{e}^{-(x-X)^2/2\delta A}}{(2\pi \delta A)^{d/2}} \right]. \tag{31}$$

We substitute this ansatz in the Bethe free energy (12) and determine the variational parameters A and δ by its extremization. In the following we will use the definition $\gamma_A(x) = \mathrm{e}^{-x^2/2A}/(2\pi A)^{d/2}$. Substituting the expressions above in (12), we obtain the following results:

$$\begin{aligned} S_{\mathrm{link}} &= \log[m^{-d/2}[2\pi(1+\delta)A]^{d(1-m)/2}], \\ S_{\mathrm{site}} &= \log[m^{(1-z)d/2} z^{(1-m)d/2} (2\pi\delta A)^{-(1-m)(1-z)d/2}]. \end{aligned} \tag{32}$$

Note that S_{box} does not depend on δ. Therefore we first write the contribution of S_{link} and S_{site} and optimize with respect to δ:

$$S_{\mathrm{site}} - z S_{\mathrm{link}} = -\frac{d}{2}(1-m)\log(2\pi A) + \frac{d}{2}\log m + \frac{d}{2}(1-m)\log\left[\frac{z\delta^{z-1}}{(1+\delta)^z}\right]. \tag{33}$$

The optimization is straightforward and gives $\delta = z-1$ as expected from the first equation of (6). The optimized result is

$$S_{\mathrm{site}} - z S_{\mathrm{link}} = -\frac{d}{2}(1-m)\log(2\pi A) + \frac{d}{2}\log m + \frac{d}{2}(1-m)(z-1)\log\left[1 - \frac{1}{z}\right]. \tag{34}$$

The last term to be computed is S_{box}, which has the form

$$S_{\mathrm{box}} = \log \int \mathrm{d}X_1 \cdots \mathrm{d}X_p \left[\int \mathrm{d}x_1 \cdots \mathrm{d}x_p \, \gamma_A(x_1 - X_1) \cdots \gamma_A(x_p - X_p) \chi(x_1, \ldots, x_p) \right]^m. \tag{35}$$

Unfortunately this cannot be computed exactly and we have to resort to further approximations.

5.1. Small cage expansion, first order

The small cage expansion proceeds as follows [5]. First we assume that m is an integer and write S_{box} as

$$S_{\text{box}} = \log \int d\bar{x}_1 \cdots d\bar{x}_p \rho(\bar{x}_1) \cdots \rho(\bar{x}_p) \prod_{i<j}^{1,p} \bar{\chi}(\bar{x}_i, \bar{x}_j), \tag{36}$$

where $\bar{x} = (x_1, \ldots, x_m)$ is the coordinate of a 'molecule' made of m particles, $\bar{\chi}(\bar{x}, \bar{y}) = \prod_{a=1}^m \chi(x_a, y_a)$, and $\rho(\bar{x}) = \int dX \prod_{a=1}^m \gamma_A(x_a - X)$. Observing that $\int dx_2 \cdots dx_m \, \rho(\bar{x}) = 1$, we write

$$S_{\text{box}} = \log \int d\bar{x}_1 \cdots d\bar{x}_p \, \rho(\bar{x}_1) \cdots \rho(\bar{x}_p) \prod_{i<j}^{1,p} [\bar{\chi}(\bar{x}_i, \bar{x}_j) - \chi(x_{1i}, x_{1j}) + \chi(x_{1i}, x_{1j})]$$

$$\sim \log \left[\int dx_{11} \cdots dx_{1p} \prod_{i<j}^{1,p} \chi(x_{1i}, x_{1j}) \right.$$

$$\left. + \sum_{i<j}^{1,p} \int dx_{11} \cdots dx_{1p} \left(\prod_{i'<j'}^{1,p} \chi(x_{1i'}, x_{1j'}) \right) Q(x_{1i} - x_{1j}) \right], \tag{37}$$

where we omitted the second order in the development in series of $\bar{\chi} - \chi_1$ and we defined

$$Q(x-y) = \int dx_1 \cdots dx_m \, dy_1 \cdots dy_m \, \rho(\bar{x}) \rho(\bar{y}) \left[\prod_{a=2}^m \chi(x_a, y_a) - 1 \right]. \tag{38}$$

In [5] it is shown that the second order gives a contribution $O(A)$ and that at lowest order (see appendix C3 of [5]) $Q(r) = 2\sqrt{A} Q_0(m) \delta(r - D)$, where $Q_0(m)$ is a function of m defined in [5] as

$$Q_0(m) = \int_{-\infty}^{\infty} [\Theta(t)^m - \Theta(t)]; \qquad \Theta(t) = \frac{1}{2}[1 + \text{erf}(t)] = \frac{1}{\sqrt{\pi}} \int_{-\infty}^{t} dx \, e^{-x^2}. \tag{39}$$

We get then

$$S_{\text{box}} \sim \log Z_p^0 + \frac{p(p-1)}{2} \int dx \, dy \, Q(x-y) g_0^p(x-y)$$

$$= \log Z_p^0 + \frac{p(p-1)}{2} \frac{2d\sqrt{A}}{D} Q_0(m) g_p^0(D) V_d(D), \tag{40}$$

and collecting all the terms we get

$$S(m) = \frac{d}{2}(m-1)\log(2\pi A) + \frac{d}{2}\log m + \frac{d}{2}(1-m)(z-1)\log\left[1 - \frac{1}{z}\right]$$

$$+ \frac{z}{p}\log Z_p^0 + \frac{z(p-1)}{2}\frac{2d\sqrt{A}}{D}Q_0(m)g_p^0(D)V_d(D). \tag{41}$$

Optimization with respect to A gives

$$\sqrt{A^*} = D\frac{1-m}{Q_0(m)}\frac{1}{z(p-1)V_d(D)g_p^0(D)}, \tag{42}$$

and

$$S(m) = \frac{d}{2}(m-1)\log(2\pi A^*) + \frac{d}{2}\log m + d(1-m) + \frac{d}{2}(1-m)(z-1)\log\left[1-\frac{1}{z}\right]$$
$$+ \frac{z}{p}\log Z_p^0. \tag{43}$$

In particular, using the results $Q_0(m \to 0) \sim \sqrt{\pi/4m}$ and $Q_0(m \sim 1) = Q_0 \times (1-m)$ with $Q_0 = 0.638$ [5], one can show that this expression trivially reduces to the RS entropy (11) for $m = 1$, and that

$$\Sigma_j = \lim_{m \to 0} S(m) = -d\log\left[\frac{2\sqrt{2}D}{z(p-1)V_d(D)g_p^0(D)}\right] + d + \frac{d}{2}(z-1)\log\left[1-\frac{1}{z}\right] + \frac{z}{p}\log Z_p^0,$$

$$\Sigma_{\rm eq} = -\lim_{m \to 1} m^2 \partial_m[S(m)/m] = -\frac{d}{2}\log\frac{2\pi}{e} - d\log\left[\frac{D}{z(p-1)V_d(D)g_p^0(D)Q_0}\right]$$
$$+ \frac{d}{2}(z-1)\log\left[1-\frac{1}{z}\right] + \frac{z}{p}\log Z_p^0.$$

5.2. Results for $p = 2$, any dimension

For $p = 2$ we have trivially $Z_2^0 = 1 - V_d(D)$ and $g_2^0(x,y) = \chi(x,y)/Z_2^0$, therefore $g_2^0(D) = 1/Z_2^0$. We get

$$S(m) = \frac{d}{2}(m-1)\log\left[\frac{2\pi D^2(1-V_d(D))^2}{z^2 V_d(D)^2}\frac{(1-m)^2}{Q_0(m)^2}\right] + \frac{d}{2}\log m$$
$$+ d(1-m) + \frac{d}{2}(1-m)(z-1)\log\left[1-\frac{1}{z}\right] + \frac{z}{2}\log[1-V_d(D)], \tag{44}$$

and

$$\Sigma_j = \lim_{m \to 0} S(m) = -\frac{d}{2}\log\left[\frac{8D^2(1-V_d(D))^2}{z^2 V_d(D)^2}\right] + d + \frac{d}{2}(z-1)\log\left[1-\frac{1}{z}\right]$$
$$+ \frac{z}{2}\log[1-V_d(D)],$$

$$\Sigma_{\rm eq} = -\lim_{m \to 1} m^2 \partial_m[S(m)/m] = -\frac{d}{2}\log\left[\frac{2\pi D^2(1-V_d(D))^2}{z^2 V_d(D)^2 Q_0^2}\right] + \frac{d}{2}$$
$$+ \frac{d}{2}(z-1)\log\left[1-\frac{1}{z}\right] + \frac{z}{2}\log[1-V_d(D)],$$

and $D_{\rm K}$ is defined by $\Sigma_{\rm eq} = 0$ while $D_{\rm GCP}$ is defined by $\Sigma_j = 0$. The results are reported in figure 3.

5.3. Results for $d = 1$, any p

Also in $d = 1$ the integrations can be performed for all p. We get

$$Z_p^0 = [1-pD]^{p-1}, \qquad g_p^0(D) = \frac{1}{1-pD}. \tag{45}$$

Figure 3. Special values of the sphere radius as functions of z at $p = 2$ for different values of d in the Gaussian approximation: D_{RS} beyond which the RS solution becomes unstable, D_{GCP} where the pressure diverges, and D_{K} where the Kauzmann transition takes place. When $D_{\mathrm{K}} < D_{\mathrm{RS}}$ the transition is necessarily first order.

Then

$$S(m) = \frac{1}{2}(m-1)\log\left[\frac{\pi(1-pD)^2}{4z^2(p-1)^2}\frac{(1-m)^2}{Q_0(m)^2}\right] + \frac{1}{2}\log m$$
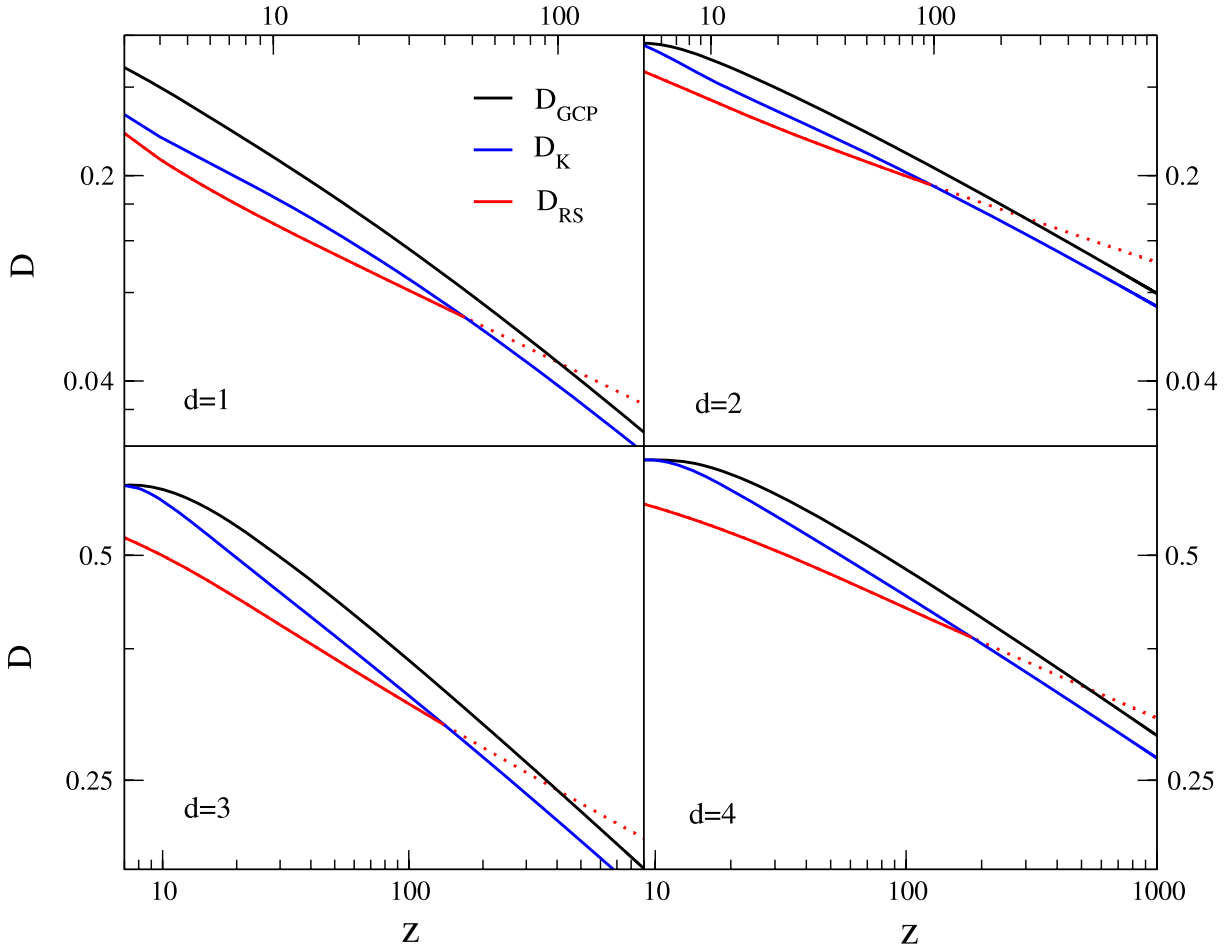$$+ (1-m) + \frac{1}{2}(1-m)(z-1)\log\left[1-\frac{1}{z}\right] + \frac{z(p-1)}{p}\log(1-pD), \qquad (46)$$

and

$$\Sigma_j = -\frac{1}{2}\log\left[\frac{2(1-pD)^2}{z^2(p-1)^2}\right] + 1 + \frac{1}{2}(z-1)\log\left[1-\frac{1}{z}\right] + \frac{z(p-1)}{p}\log(1-pD),$$

$$\Sigma_{\mathrm{eq}} = -\frac{1}{2}\log\left[\frac{\pi(1-pD)^2}{2z^2(p-1)^2Q_0^2}\right] + \frac{1}{2} + \frac{1}{2}(z-1)\log\left[1-\frac{1}{z}\right] + \frac{z(p-1)}{p}\log(1-pD).$$

The results are reported in figure 4.
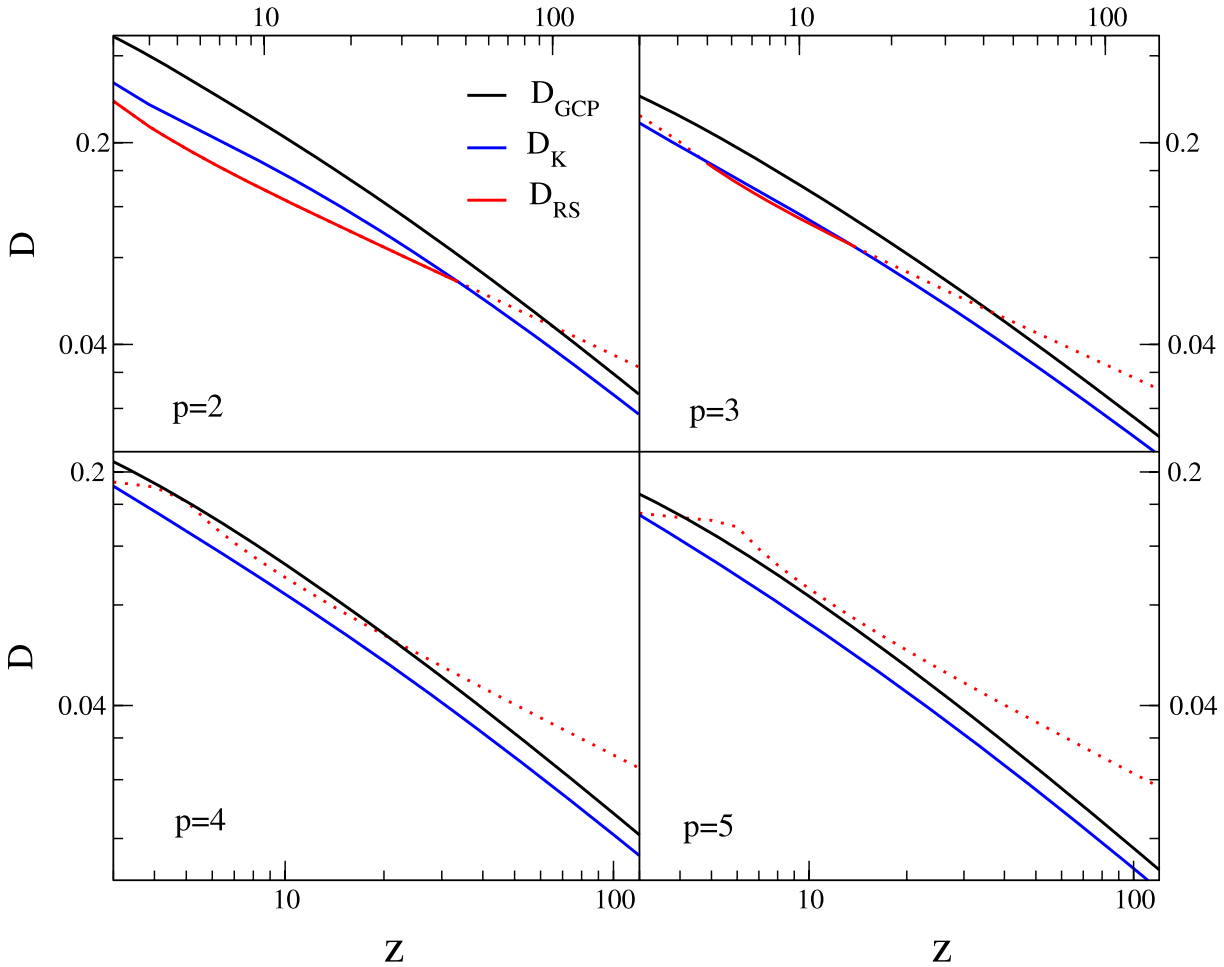
Figure 4. D_{RS}, D_{GCP} and D_K as functions of z for different values of p at $d = 1$ in the Gaussian approximation.

6. The delta approximation

In this section we introduce another variational approximation scheme, that we shall call the 'delta approximation'. The motivation is that within the Gaussian ansatz, $A \to 0$ at jamming; therefore both $\psi(x)$ and $\varphi(x)$ become delta functions in this limit. We would therefore like to compute the free energy directly for delta function fields; we expect this to give a simpler expression of the free energy, that should be good close to jamming. The problem is that the Gaussian expressions are divergent for $A \to 0$ unless m also goes to zero proportionally to A. This is due to the fact that both fields $\psi(x)$ and $\varphi(x)$ become delta functions for $A \to 0$. We therefore construct here a different approximation by eliminating the field $\varphi(x)$ and making a delta function ansatz only for the field $\psi(x)$; in this way the field $\varphi(x)$ is computed exactly and in particular it is not a delta function.

One can show in general that by using equations (13), one can eliminate the field $\varphi(x)$ and the replicated entropy can be equivalently written as

$$S(m) = S_{\text{site}'} - \frac{z(p-1)}{p} S_{\text{box}}, \tag{47}$$

where S_{box} is defined as in equation (12) and

$$
\begin{aligned}
S_{\text{site}'} = \log \int \mathrm{d}\mathcal{P}[\psi_1^1] \cdots \mathrm{d}\mathcal{P}[\psi_{p-1}^z] \\
\times \left[\int \mathrm{d}x \prod_{k=1}^z \int \mathrm{d}x_1^k \cdots \mathrm{d}x_{p-1}^k \psi_1^k(x_1^k) \cdots \psi_{p-1}^k(x_{p-1}^k) \chi(x, x_1^k, \ldots, x_{p-1}^k) \right]^m \\
\equiv \log \langle Z_{\text{site}'}^m \rangle.
\end{aligned}
\tag{48}
$$

The 'delta approximation' is then based on the following ansatz for $\mathcal{P}(\psi)$:

$$
\mathcal{P}[\psi] = \int \mathrm{d}X\, \delta[\psi(x) - \delta(x - X)],
\tag{49}
$$

namely on each site i the probability of the variable x_i is a delta function centered in an i.i.d. random point. Under approximation (49), the replicated entropy becomes

$$
\begin{aligned}
S(m) &= \log \int \mathrm{d}X_1^1 \cdots \mathrm{d}X_{p-1}^z \left(\int \mathrm{d}x \prod_{k=1}^z \chi(x, X_1^k, \ldots, X_{p-1}^k) \right)^m \\
&\quad - \frac{z(p-1)}{p} \log \int \mathrm{d}X_1 \cdots \mathrm{d}X_p \chi(X_1, \ldots, X_p) \\
&= \log \int \left(\prod_{k=1}^z \mathrm{d}X_1^k \cdots \mathrm{d}X_{p-1}^k \chi(X_1^k, \ldots, X_{p-1}^k) \right) v_{z(p-1)}(X_1^1 \cdots X_{p-1}^z)^m \\
&\quad - \frac{z(p-1)}{p} \log Z_p^0,
\end{aligned}
\tag{50}
$$

recalling the definition of v_n in equation (5). Introducing the normalized measure of n spheres in a unit box,

$$
\mathrm{d}\mu(x_1 \cdots x_n) = \frac{\mathrm{d}x_1 \cdots \mathrm{d}x_n\, \chi(x_1 \cdots x_n)}{Z_n^0},
\tag{51}
$$

we can rewrite $S(m)$ given in equation (50) in the equivalent form

$$
\begin{aligned}
S(m) &= \log \int \left(\prod_{k=1}^z \mathrm{d}\mu\left(X_1^k \cdots X_{p-1}^k\right) \right) \left[v_{z(p-1)}(X_1^1, \ldots, X_{p-1}^z) \right]^m + z \log Z_{p-1}^0 \\
&\quad - \frac{z(p-1)}{p} \log Z_p^0.
\end{aligned}
\tag{52}
$$

In the following we study this expression for several specific values of p and d. In this section we will derive the expressions for the complexity, and in section 8 we will present the results together with a comparison with numerical resolution of the cavity equations. Note that for $m = 1$ one can easily show that $S(m)$ given above is equal to the RS entropy (11), which is an important requirement for the consistency of this approximation.

6.1. One dimension

6.1.1. Results for $p = 2$. We first consider the simplest case, namely one spatial dimension and only two-particles-in-a-box interactions ($p = 2$). Since $Z_1^0 = 1$ and $Z_2^0 = (1 - 2D)$, we get

$$S(m) = \log \int \prod_{i=1}^{z} dX_i \, [v_z(X_1 \cdots X_z)]^m - \frac{z}{2} \log(1 - 2D). \tag{53}$$

We have therefore to compute the probability distribution $P_z(v)$ of the void space left in $[0, 1]$ for the insertion of a new particle, after having put z particles in random positions $\{X_i\}$. Then we have

$$S(m) = \log \int_0^{1-2D} dv \, P_z(v) \, v^m - \frac{z}{2} \log(1 - 2D). \tag{54}$$

Note that v ranges from 0 (no void space) to $1 - 2D$ (in the limiting case where all points X_i coincide), and we expect that $P_z(v) = p_0 \delta(v) + P_z^{\mathrm{reg}}(v)$ since a finite fraction of the configurations have zero void space at large enough D. Since the delta function does not contribute to $S(m)$, we will omit it from now on.

In order to estimate $P_z(v)$, we can make the assumption that whenever $v > 0$, there is only one hole large enough to contribute to v (i.e. a hole whose length is larger than $2D$). The function $P_z(v)$ can then be easily evaluated in the following way. The hole that contributes to v must have length $2D + v$, and must be delimited by two particles that we can choose in $z(z-1)$ different ways, since the particles are distinguishable. We can put the first particle in $x_1 = 0$ and the second in $x_2 = 2D + v$ (integration over x_1 can be omitted since it gives a factor of 1, the length of the box). The remaining $z - 2$ particles must be in the space between x_2 and 1, therefore giving a contribution $(1 - 2D - v)^{z-2}$. Therefore, within the one-hole approximation, we get $P_z(v) = z(z - 1)(1 - 2D - v)^{z-2}$. We notice that the total probability of $v > 0$ must be smaller then one since some configurations might have $v = 0$. This gives the condition

$$\int_0^{1-2D} dv \, P_z(v) = z(1 - 2D)^{z-1} \leq 1 \Rightarrow D \geq (1 - z^{-1/(z-1)})/2, \tag{55}$$

which gives an estimate of the limits of validity of the one-hole approximation.

Plugging the result for $P_z(v)$ into equation (54), we get an approximate formula for the replicated free energy which depends on z and D:

$$S(m) = \log \left(\frac{\Gamma(z+1)\Gamma(m+1)}{\Gamma(z+m)} \right) + \left(m - 1 + \frac{z}{2} \right) \log(1 - 2D). \tag{56}$$

Recall that $\Sigma_{\mathrm{eq}} = -[m^2 \partial_m (S(m)/m)]|_{m=1}$ and that D_{K} is the point where the latter quantity vanishes. We get

$$\Sigma_{\mathrm{eq}} = \sum_{q=2}^{z} \frac{1}{q} + \frac{z-2}{2} \log(1 - 2D), \qquad D_{\mathrm{K}} = \frac{1}{2}[1 - e^{-2/(z-2) \sum_{q=2}^{z}(1/q)}]. \tag{57}$$

On the other hand, $\Sigma_j = S(m = 0)$ and it vanishes at the close packing diameter D_{GCP}. We get

$$\Sigma_j = \log(z) + \frac{z-2}{2}\log(1-2D), \qquad D_{\mathrm{GCP}} = \tfrac{1}{2}[1 - z^{-2/(z-2)}]. \qquad (58)$$

The complexity curve can be obtained explicitly, using $\Sigma = -m^2\partial_m(S(m)/m)$ and $s = \partial_m S(m)$, which gives the parametric representation

$$
\begin{aligned}
s &= \log(1-2D) - \sum_{q=1}^{z-1}\frac{1}{m+q}, \\
\Sigma &= \frac{z-2}{2}\log(1-2D) + \log\left(\frac{\Gamma(z+1)\Gamma(m+1)}{\Gamma(z+m)}\right) + m\sum_{q=1}^{z-1}\frac{1}{m+q}.
\end{aligned}
\qquad (59)
$$

One can check easily that both critical diameters D_{K} and D_{GCP} are well within the region of validity of the one-hole approximation given by equation (55), and they scale as $D_{\mathrm{K}}, D_{\mathrm{GCP}} \sim \log z/z$ in the large connectivity limit. The values of D_{K} and D_{GCP} can be compared to the stability of the RS solution (which scales as $D_s \sim 1/\sqrt{z}$).

6.1.2. Results for $p = 3$. We now consider the three-particles-in-a-box case $p = 3$, still for $d = 1$. Since $Z_2^0 = 1 - 2D$ and $Z_3^0 = (1 - 3D)^2$, we get from equation (52)

$$S(m) = \log\int_0^{1-3D}\mathrm{d}v\, P_{2,z}(v)\,v^m + z\log(1-2D) - \frac{4z}{3}\log(1-3D), \qquad (60)$$

where now $P_{2,z}(v)$ is the probability distribution of the void space in $[0,1]$ for the insertion of a new particle, after having thrown at random z pairs of particles, each pair being at distance larger than D. The latter ranges from 0 (no void space) to $1 - 3D$ (in the case where each pair is exactly at distance D and superposed to all the others).

Within the same one-hole approximation, we can approximate $P_{2,z}(v)$ as follows. The hole must have length $L = 2D + v$. We have to distinguish between two different situations: (i) the hole is made by the same couple of particles; (ii) the hole is made by two different couples. In the case (i) we have z ways of choosing the couple. We fix then one of the two particles of the couple in 0 and the other one in L (which gives an extra factor 2). Finally the other $z - 1$ couples of particles must be in the interval $[L, 1]$ with the conditions that they are pairwise compatible, which gives a factor $f(L, D) = \int_L^1 \mathrm{d}x \int_L^1 \mathrm{d}y\, \chi(x, y) = (1 - L - D)^2$ for each pair. With this definition the contribution due to the same couple finally reads $2zf(L, D)^{z-1}$. In the case (ii), instead, we can fix one particle of one couple in 0 (we have $2z$ ways to choose it) and one particle of another couple in L (we have $2(z - 1)$ ways of choosing it). The free particle of the first couple must be in $[L, 1 - D]$, due to the condition that it is compatible with its partner which has been fixed in 0. This gives a contribution $(1 - L - D)$. An analogous contribution comes from the free particle of the second couple, which must be in the interval $[L + D, 1]$. The other $z - 2$ couples must be in the interval $[L, 1]$ and must satisfy the compatibility condition, and therefore give a contribution $f(L, D)^{z-2}$. The sum of the two contributions is $(4z^2 - 2z)(1 - L - D)^{2(z-1)}$, and it has to be normalized by the total

integral $(1 - 2D)^z$; going back to $v = L - 2D$ we get

$$P_{2,z}(v) = \frac{2z(2z - 1)(1 - v - 3D)^{2(z-1)}}{(1 - 2D)^z}. \tag{61}$$

As in the previous case we get the condition

$$\int_0^{1-3D} dv\, P_{2,z}(v) = \frac{2z(1 - 3D)^{2z-1}}{(1 - 2D)^z} \le 1, \tag{62}$$

which gives a lower limit of validity in D of the one-hole approximation.

Plugging this result into equation (60) we get for the replicated entropy

$$S(m) = \log\left[\frac{\Gamma(m+1)\Gamma(1+2z)}{\Gamma(m+2z)}\right] + \left(m - 1 - \frac{2z}{3}\right)\log(1 - 3D), \tag{63}$$

from which we get

$$\Sigma_{\text{eq}} = \sum_{q=2}^{2z}\frac{1}{q} + \frac{2z-3}{3}\log(1 - 3D), \qquad D_K = \tfrac{1}{3}[1 - e^{-(3/2z-3)\sum_{q=2}^{2z}(1/q)}], \tag{64}$$

and

$$\Sigma_j = \log(2z) + \frac{2z-3}{3}\log(1 - 3D), \qquad D_{\text{GCP}} = \tfrac{1}{3}[1 - (2z)^{-3/(2z-3)}]. \tag{65}$$

We checked that both D_{GCP} and D_K are well within the region of validity of the one-hole approximation; actually, the value of the left-hand side of equation (62) never exceeds 0.1. Again, D_{GCP} and D_K are found to scale as $2\log z/z$ for large z.

6.1.3. Conjecture for arbitrary p (2, 3, ..., ∞). A comparison of equations (57) and (63) and of equations (58) and (64) allows us to guess the form for general p:

$$\begin{aligned}
\Sigma_{\text{eq}} &= \sum_{q=2}^{(p-1)z}\frac{1}{q} + \frac{(p-1)z - p}{p}\log(1 - pD), \\
D_K &= \frac{1}{p}\left[1 - e^{-p/((p-1)z-p)\sum_{q=2}^{(p-1)z}(1/q)}\right], \\
\Sigma_j &= \log((p-1)z) + \frac{(p-1)z - p}{p}\log(1 - pD), \\
D_{\text{GCP}} &= \frac{1}{p}[1 - ((p-1)z)^{-p/((p-1)z-p)}].
\end{aligned} \tag{66}$$

However we did not attempt to provide a proof of this conjecture.

6.2. Two dimensions

In the $d = 2$ case we cannot compute $S(m)$ analytically and we must resort to a numerical evaluation. The numerical algorithm consists in writing a routine that is able to compute the void space v_n, defined in equation (5), left by n discs centered in a set of positions $\{X\}$. We used an adaptation of the algorithm described in [24] that works as follows.

- We start by a grid of squares of side $\Delta \ll D$ (typically $\Delta = 1/100$). These squares are considered as particular cases of convex polygons.

- We add discs $X_1 \cdots X_n$ sequentially.

- Each time a disc is added, we check if a given polygon is entirely contained in the disc. In this case it is removed from the grid.

- Next we consider the polygons that intersect the boundary of the new disc. We approximate the boundary of the void space left in the old polygon by a new polygon, by approximating the boundary of the disc by a straight line (which is reasonable if $\Delta \ll D$, with error $\mathrm{O}(\Delta/D)^2$). The new polygon replaces the old one in the grid.

- This construction is iterated until all discs have been placed. The area of the polygons that survived is computed easily using equation (1) of [24], and it gives the void space v_n.

The void space has to be averaged over the distribution $\prod_{i=1}^{z} \mathrm{d}\mu(X_1^i \cdots \mathrm{d}X_{p-1}^i)$, hence we must sample a configuration of $p - 1$ spheres in a box (and do this z times independently). This can be easily done for $p = 2$ (one sphere, flat distribution) and $p = 3$ (put one sphere in the center of the box, draw a second sphere outside it, then translate randomly both spheres).

A correct sampling gives access to the void space distribution $P(v)$, that has the form $P(v) = p_0 \delta(v) + P^{\mathrm{reg}}(v)$, as in one dimension. In the following we omit the delta term and only consider $P^{\mathrm{reg}}(v)$, which therefore is not normalized to one (its integral gives the probability that $v > 0$). From this we can compute equation (52) as we did in one dimension:

$$S(m) = \log \int \mathrm{d}v\, P(v)\, v^m + z \log Z_{p-1}^0 - \frac{z(p-1)}{p} \log Z_p^0. \tag{67}$$

Similarly we get, using the relation $\int \mathrm{d}v\, P(v)\, v = \langle v \rangle = (Z_p^0/Z_{p-1}^0)^z$ (which can be easily checked and also serves as a check of the correct sampling of $P(v)$),

$$\Sigma_{\mathrm{eq}} = \frac{z}{p} \log Z_p^0 - \left(\frac{Z_{p-1}^0}{Z_p^0} \right)^z \int \mathrm{d}v\, P(v)\, v \log v,$$
$$\Sigma_j = \log \int \mathrm{d}v\, P(v) + z \log Z_{p-1}^0 - \frac{z(p-1)}{p} \log Z_p^0. \tag{68}$$

Therefore both Σ_{eq} and Σ_j can be computed directly from $P(v)$; from them we can determine the transition points D_{K} and D_{GCP}.

7. Numerical solution of the equations

In the previous sections we described two analytical approximate methods yielding the phase diagram of the model. Beyond these analytical approaches, one can also develop some algorithms to solve the functional self-consistent 1RSB equations numerically. In this section we explain how it is possible to implement a numerical procedure to solve equations (13) in the 1RSB phase for each value of the connectivities, z and p, of the diameter D, of the 1RSB parameter m and, in principle, of the spatial dimension d (in practice, numerical solutions can only be achieved in one and two dimensions). In order to do that we need representations of the cavity fields $\varphi(x)$ and $\psi(x)$, and of the distributions $\mathcal{P}[\varphi]$ and $\mathcal{P}[\psi]$, which can be treated by a computer.

As far as the cavity fields are concerned, the simplest possibility is to discretize the volume $[0,1]^d$ where the functions $\varphi(x)$ and $\psi(x)$ are defined using a regular hyper-cubic grid with q bins per side of size $1/q$. For instance, in one dimension we discretize the interval $[0,1]$ in q slices of length $1/q$, and in two dimension we discretize the square box on a square lattice of $q \times q$ points.

The coordinate in the box can assume a discrete set of values, $\vec{i}/q$, with $\vec{i}$ being a d-dimensional vector whose components are integers between 0 and $q-1$, identifying the coordinate of the position of the center of the sphere in the box. If the position of the center of the sphere occupies a given site of the grid $\vec{i}$, then all other sites of the lattice that are at Euclidean distance from $\vec{i}$ smaller than the diameter of the sphere D cannot be occupied by the center of another sphere (we call this number n_D). The volume of the sphere in the discretized version of the model can be estimated as $V_s = n_D/(2q)^d$, and the packing fraction as $\varphi = pV_s = pn_D/(2q)^d$. Since in the continuum limit $V_s = V_d(1)(D/2)^d$, we can then define an effective diameter as $D_{\text{eff}} = (1/q)[n_D/V_d(1)]^{1/d}$. Note that in general $D_{\text{eff}} \neq D$, and we take D_{eff} as representative of the sphere diameter in the continuum limit. In particular, by symmetry, in $d = 1$ the number of excluded sites always has the form $n_D = 1 + 2a$ for integer a, and one has

$$D_{\text{eff}} = \frac{1+2a}{2q}. \tag{69}$$

In $d = 2$ the parameter n_D depends in an irregular manner on the choice of D (since the square lattice we use breaks the spherical symmetry) and one has in general

$$D_{\text{eff}} = \frac{1}{q}\sqrt{\frac{n_D}{\pi}}. \tag{70}$$

In the discretized version, the fields $\varphi(x)$ and $\psi(x)$ are vectors of q^d components (such that the sum of all components is equal to one), and the cavity equations, equation (6), become a set of coupled algebraic equations for the q^d components of the cavity fields, which can be easily solved numerically (of course, the numerical complexity of this step grows linearly with the number of components of the cavity fields, q^d).

Note that the discretized version of the model is a generalization of a very important optimization problem known as the 'random graph coloring' problem, where the number of colors corresponds to the number of components of the cavity fields q^d. In particular, for $n_D = 0$ and $p = 2$ we recover the standard q-coloring problem, which has been deeply studied in the past few years, and whose properties and phase diagram are known in great detail [25].

The continuum limit of the model is, of course, recovered for $q \to \infty$. As a consequence, in order to make sure that the numerical results are reliable and that they are not affected by the discretization, we solve numerically the 1RSB equations using several values of q, and analyze the scaling properties of the numerical solutions with the number of bins. Moreover, one should note that for $d > 1$, partitioning the box using a hyper-cubic grid breaks the spherical symmetry down to some discrete symmetry. This makes the scaling towards the continuum limit in two dimensions more problematic than in one dimension (also because, due to the fact that the complexity of the numerical algorithm grows as q^d, we are limited to smaller values of q for $d = 2$).

Other numerical representations of the cavity fields were also possible. For instance, as $\varphi(x)$ and $\psi(x)$ are periodic functions in the interval $[0,1]^d$, we could have performed a Fourier transformation of the recurrence equations keeping all the components up to a certain momentum, yielding a finite set of coupled algebraic equations for the Fourier coefficients of the cavity fields (similarly to what we did in section 4 to study the RS stability). However, it turns out that this strategy is not efficient in the most interesting region of the phase diagram, namely at high packing fraction where a 1RSB glass transition is found. Indeed here the cavity fields become extremely peaked (this is also the reason why the Gaussian and the delta approximation work very well), and the momentum cutoff needed to get accurate results becomes too large to be handled.

Another possibility we could have employed was to represent the fields as a population of delta functions, e.g. $\varphi(x) = \sum_\alpha c_\alpha \delta(x - x_\alpha)$. This strategy, which has the advantage that one does not need to discretize the space, has, on the other hand, the disadvantage that at each step of the iterative procedure, in order to generate a new field, one has to sample uniformly one point in the free space available for the insertion of a new particle, given the position of $z(p-1)$ neighboring particles in the box. This is trivial in $d = 1$, however in that case the discretized procedure works already well enough. In $d = 2$, this could be done using the algorithm described in section 6.2. However this algorithm is too slow to be used efficiently for this scope. Therefore in the following we will not explore further this representation.

7.1. The population dynamics algorithm

Now, once that we dispose of the discretized representation of the cavity fields, we need to be able to implement a computational strategy to solve the 1RSB functional self-consistent equations, equations (13), for any values of the connectivities, z and p, of the diameter of the spheres, D, and of the 1RSB parameter m. This step is quite standard in the context of the cavity method, and goes under the name of 'population dynamics algorithm' [23]. The idea is to represent the probability distributions $\mathcal{P}[\varphi]$ and $\mathcal{P}[\psi]$ as populations of $\mathcal{M}$ representative cavity fields with some weights:

$$\mathcal{P}[\varphi] = \sum_{\alpha=1}^{\mathcal{M}} z_\varphi^\alpha \, \delta[\varphi(x) - \varphi_\alpha(x)], \qquad \text{and} \qquad \mathcal{P}[\psi] = \sum_{\alpha=1}^{\mathcal{M}} z_\psi^\alpha \, \delta[\psi(x) - \psi_\alpha(x)]. \tag{71}$$

As previously discussed, we need to consider only the translationally invariant solution of equations (13) in order to describe the glassy phase. A solution $\mathcal{P}[\psi(x)]$ is translationally invariant if the property $\mathcal{P}[\psi(x+s)] = \mathcal{P}[\psi(x)]$ holds for any $s \in [0,1]^d$, where $\psi(x+s)$ is an arbitrary translation (taking into account periodic boundary conditions) of $\psi(x)$.

Since we represent the probability distribution $\mathcal{P}[\psi]$ by a set of representative samples $\psi_\alpha(x)$, it is very easy to implement translational invariance. In principle, we would like to impose that if $\psi_\alpha(x)$ is one of the samples, then any translation of it is also contained in the set of samples with the same weight. But this is just equivalent to doing the following: at each time we use a given sample $\psi(x)$ as a representative of $\mathcal{P}[\psi]$, we apply to it a 'random shift', namely we extract a vector s uniformly in $[0,1]^d$ and we translate $\psi(x)$ by s. In this way we impose translational invariance by hand.

The population dynamics algorithm works in the following way.

(1) Pick at random $p-1$ fields ψ_i from the population $\mathcal{P}[\psi]$, according to their weights z_ψ^α. Apply a random shift with flat probability in $[0,1]^d$ to each of the cavity fields.

(2) Using equations (6), compute the new cavity field φ, along with its weight z_φ, which is given by the normalization in equations (14) to the power m, according to equations (13). Note that at high density, in the 1RSB phase, the cavity fields become extremely peaked. This implies that there exist some configurations of the $p-1$ fields ψ_i for which the new field φ is zero everywhere in $[0,1]^d$. In this case the corresponding weight is zero and we have to reject it and restart the procedure. These events, which can cause a major slowing down of the algorithm, are called 'rejection events'.

(3) Repeat (1) and (2) $\mathcal{M}$ times, until a whole new population $\mathcal{P}_{\text{new}}[\varphi]$ is generated, and replace the old population with the new one (this kind of update is called in the context of the population dynamics algorithm a 'parallel update').

(4) Apply steps (1)–(3) using the population $\mathcal{P}[\varphi]$ to generate a new $\mathcal{P}_{\text{new}}[\psi]$.

(5) Repeat steps (1)–(4) until convergence, namely until the populations $\mathcal{P}[\psi]$ and $\mathcal{P}[\varphi]$ are stationary.

Once this process has converged, we can compute the average values of the link, the site and the box contributions to the 1RSB entropy, equation (12), from which one can obtain the complexity $\Sigma(m)$. This allows us to determine the equilibrium value of $m^\star$ inside the 1RSB glassy phase as the point where $S(m)$ has a minimum [9]. In practice, instead of computing the replicated entropy using equations (12), we can use another and equivalent formula (derived below) which is more advantageous from a numerical point of view. Indeed, using equation (6) we can easily obtain the following relations (we omit the arguments of the functions Z):

$$Z_{\text{link}} = \frac{Z_{\text{box}}}{Z_\varphi} = \frac{Z_{\text{site}}}{Z_\psi}. \tag{72}$$

Using these and equations (13), one can rewrite the total and internal entropy as

$$S(m) = \left(1 - z + \frac{z}{p}\right) S_{\text{link}} + \frac{z}{p} S_\varphi + S_\psi, \qquad s(m) = \left(1 - z + \frac{z}{p}\right) s_{\text{link}} + \frac{z}{p} s_\varphi + s_\psi. \tag{73}$$

The computation of $S_\varphi = \log\langle Z_\varphi^m \rangle$ and $S_\psi = \log\langle Z_\psi^m \rangle$ is numerically less involved than S_{site} and S_{box} appearing in equations (12). Moreover, these contributions can be evaluated online during steps (1)–(5) of the population dynamics algorithm described above (we have just to compute the average values of Z_φ^m and Z_ψ^m over all the $\mathcal{M}$ attempts of generating a new cavity field), without requiring the implementation of any further step.

Of course, representing the distributions $\mathcal{P}[\psi]$ and $\mathcal{P}[\varphi]$ as populations of $\mathcal{M}$ elements is an approximation which becomes exact only in the $\mathcal{M} \to \infty$ limit. On the other hand, the numerical complexity of the population dynamics algorithm grows linearly with $\mathcal{M}$. In practice one has to find a good compromise between a value of $\mathcal{M}$ small enough such that the execution time of the code stays reasonable, but large enough to avoid systematic corrections due to the finite size of the populations. In the present case, we find that $\mathcal{M} = 2^{16}$ is close to the optimal value.

Although we have produced a working version of the algorithm described above at any finite value of the 1RSB parameter m, it turned out that the execution time is too large to get accurate results in a reasonable time. However, there are two special limits, namely $m \to 1$ and $m \to 0$, which describe respectively the physics at the Kauzmann point and in the close packing regime, where some simplifications arise which allow us to perform the numerical study of the model in a more efficient way. These two limits are discussed below.

7.2. Reconstruction: the limit $m = 1$

In this section we consider the numerical solution of the 1RSB equations for $m = 1$. Recall that $S(m = 1)$ gives back the equilibrium RS entropy of the system between the dynamical transition (where a non-RS solution of the 1RSB equations appears for the first time due to the emergence of glassy metastable states) and the Kauzmann point. In this limit, using the approach introduced in [26] which goes under the name of reconstruction method, also applied in a similar context to the coloring optimization problem in [25], the self-consistent 1RSB equations can be simplified. Similarly to [25, 26], one can indeed introduce two new families of distributions over the cavity fields for each value of the variable x, defined as

$$\mathcal{R}_x[\psi] \equiv \psi(x)\mathcal{P}[\psi] \qquad \text{and} \qquad \mathcal{R}_x[\varphi] \equiv \varphi(x)\mathcal{P}[\varphi]. \tag{74}$$

Using the previous definitions, the 1RSB cavity equations, equations (13) can be rewritten in terms of these new distributions. Furthermore, imposing the translational invariance which implies that $\mathcal{R}_x[\psi(y)] = \mathcal{R}_0[\psi(y-x)]$ for all x we obtain the self-consistent recursion relation for the new distributions which read

$$\mathcal{R}_0[\psi] = \int \prod_{i=1}^{z-1} \mathrm{d}\mathcal{R}_0\,[\varphi_i]\,\delta\left[\psi(x) - \frac{1}{Z_\psi}\prod_i \varphi_i(x)\right],$$

$$\mathcal{R}_0[\varphi] = \int \mathrm{d}\mu\,(x_1\cdots x_{p-1}|0)\prod_{i=1}^{p-1}\mathrm{d}\mathcal{R}_0[\psi_i] \tag{75}$$

$$\times\;\delta\left[\varphi(y) - \frac{1}{Z_\varphi}\int\prod_j \mathrm{d}y_j\,\psi_j(y_j - x_j)\chi(y, y_1, \ldots, y_{p-1})\right],$$

where

$$\mathrm{d}\mu\,(x_1\cdots x_{p-1}|0) = \frac{\chi(0, x_1, \ldots, x_{p-1})\,\mathrm{d}x_1\cdots\mathrm{d}x_{p-1}}{Z_p^0}. \tag{76}$$

From a numerical point of view, these latter equations are much easier to solve than equations (13) for two reasons. First, no reweighting factor is present, which prevents the

population from concentrating on few cavity fields with large weight. Second, rejection events cannot occur in this case. Indeed, for example, the procedure to generate a new field φ amounts to the following.

(1) Pick at random $p-1$ fields ψ_i from the population $\mathcal{R}_0[\psi]$. Note that all the fields have the same weight in this representation.

(2) Pick $p-1$ variables $x_1, \ldots, x_{p-1}$ in the interval $[0,1]^d$ satisfying the hard sphere constraint $\chi(0, x_1, \ldots, x_{p-1})$ with a flat measure.

(3) Shift each of the $p-1$ chosen cavity fields ψ_i by x_i.

(4) Using equation (6), compute the new cavity fields φ (again, note that there is no reweighting in this case), and insert the new field randomly into the population $\mathcal{R}_0[\varphi]$ (this kind of update is called a 'serial update' and ensures a better convergence than the parallel one).

Once the populations $\mathcal{R}_0[\varphi]$ and $\mathcal{R}_0[\psi]$ have attained stationarity, we can compute the complexity of the system. Since the replicated entropy $S(m=1)$ equals the RS one, the complexity at $m=1$ is given by $\Sigma_{\mathrm{eq}} = S_{\mathrm{RS}} - s(m=1)$. The internal entropy can be evaluated using equations (15) and (13), where

$$
\begin{aligned}
\langle Z_{\mathrm{link}} \log Z_{\mathrm{link}} \rangle &= \int \mathrm{d}\mathcal{R}_0[\psi]\, \mathrm{d}\mathcal{R}_0[\varphi] \log \int \mathrm{d}y\, \psi(y)\varphi(y), \\
\langle Z_\psi \log Z_\psi \rangle &= \int \prod_{i=1}^{z-1} \mathrm{d}\mathcal{R}_0[\varphi_i] \log \int \mathrm{d}y \prod_i \varphi(y), \\
\langle Z_\varphi \log Z_\varphi \rangle &= \int \mathrm{d}\mu(x_1 \cdots x_{p-1}|0) Z_p^0 \prod_{i=1}^{p-1} \mathrm{d}\mathcal{R}_0[\psi_i] \log \int \mathrm{d}y \\
&\quad \times \prod_i \mathrm{d}y_i\, \psi_i(y_i - x_i)\chi(y, y_1, \ldots, y_{p-1}).
\end{aligned}
\tag{77}
$$

From the complexity we can determine the Kauzmann point, which corresponds to the value D_K where Σ_{eq} vanishes.

In principle this method would also allow us to determine the location of the dynamical transition, which is the first point where a non-RS solution of the 1RSB equations appears at $m=1$.

The results at $m=1$ obtained with the reconstruction method will be discussed in section 8, and compared with the analytical approximations.

7.3. Hard fields: the limit $m=0$

Also this specific limit yields a simplification of the numerical algorithm. The $m \to 0$ limit corresponds in this context to the 'close packing limit', since an inspection of the expression of the internal entropy $s(m)$ shows that it goes to $-\infty$ as $\log(m)$, and the pressure diverges as well [5]. Therefore the limit $m \to 0$ gives access to the jammed glassy states at infinite pressure [5].

The limits for m going to zero of Z_{link}^m, Z_{box}^m, and Z_{site}^m are either zero (for 'incompatible' configurations of the cavity fields) or one (for 'compatible' configurations of the cavity fields) regardless of the value of the cavity fields. As a consequence, in order to compute

the complexity (which equals the replicated entropy $S(m \to 0)$, since the internal entropy term, $ms(m)$, disappears) we are only interested in the propagation of this information.

To this aim, we introduce the 'hard' components of the cavity fields ψ_{hard} and φ_{hard}:

$$\psi_{\text{hard}}(x) = \begin{cases} 1 & \text{if } \psi(x) > 0 \\ 0 & \text{otherwise} \end{cases} \qquad \text{and} \qquad \varphi_{\text{hard}}(x) = \begin{cases} 1 & \text{if } \varphi(x) > 0 \\ 0 & \text{otherwise.} \end{cases} \tag{78}$$

These functions are defined as being equal to one for all values of x such that the cavity fields are non-vanishing regardless of their value (i.e., corresponding to a non-vanishing probability of finding a sphere with center in x), and zero otherwise. Since the reweighting factors in equations (13) do not depend on the actual value of the fields in the $m \to 0$ limit, the propagation of the hard components decouples completely from the propagation of the cavity fields and can thus be treated independently. As a consequence, the population dynamics algorithm described above can be used on the populations encoding the probability distributions of the hard fields. Once a stationary state has been reached, we can compute the complexity at $m = 0$, Σ_j, from equations (12), computing the logarithm of the average value of the fraction of attempts yielding non-vanishing values of Z_{link}, Z_{box}, and Z_{site}. Using equation (73), instead of computing $\langle Z_{\text{box}}^m \rangle$ and $\langle Z_{\text{site}}^m \rangle$, one can more easily compute $\langle Z_\psi^m \rangle$ and $\langle Z_\varphi^m \rangle$, which are given respectively by the average values of the fractions of non-rejection attempts to generate the new ψ_{hard} and φ_{hard} fields over the total number of attempts. Then we can determine the location of D_{GCP} defined as $\Sigma_j(D_{\text{GCP}}) = 0$.

The results at $m = 0$ obtained with this method will be reported in section 8, and compared with the analytical approximations.

An important *caveat* is that in principle some fields could be proportional to $\exp(-1/m)$ in the limit $m \to 0$. If this happens, then the procedure above fails since these fields give a finite contribution to the normalizations which is neither 0 nor 1. Although we could not perform a careful systematic investigation of this effect, it seems that it might happen only for values of z and p where the transition at $m = 1$ is continuous. This point surely deserves further investigation.

Note that in order to compute the correlation function in the close packing limit (see section 9) we also need to know the actual values of the cavity fields. Since the propagation of the hard components decouples completely from that of the fields themselves, one can use the population dynamics algorithm to find the solution of the 1RSB equations for the distributions of the hard fields and of the cavity fields independently (knowing that the cavity fields can only be nonzero where the hard components are equal to one), and use equation (80) to compute the pair correlation function.

8. Comparison between the numerical results and the approximations

In this section we report the results obtained from the direct numerical calculation with discretized space and we compare them with the delta and Gaussian approximations.
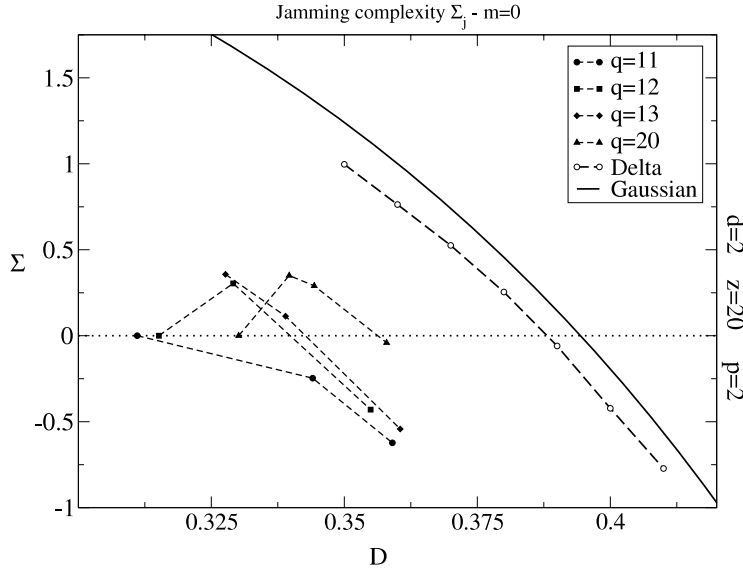
8.1. Complexity

In figure 5 we report the complexities Σ_{eq} (the complexity at $m = 1$ equal to $(1/N)$ times the logarithm of the typical number of glass states when the configurations are
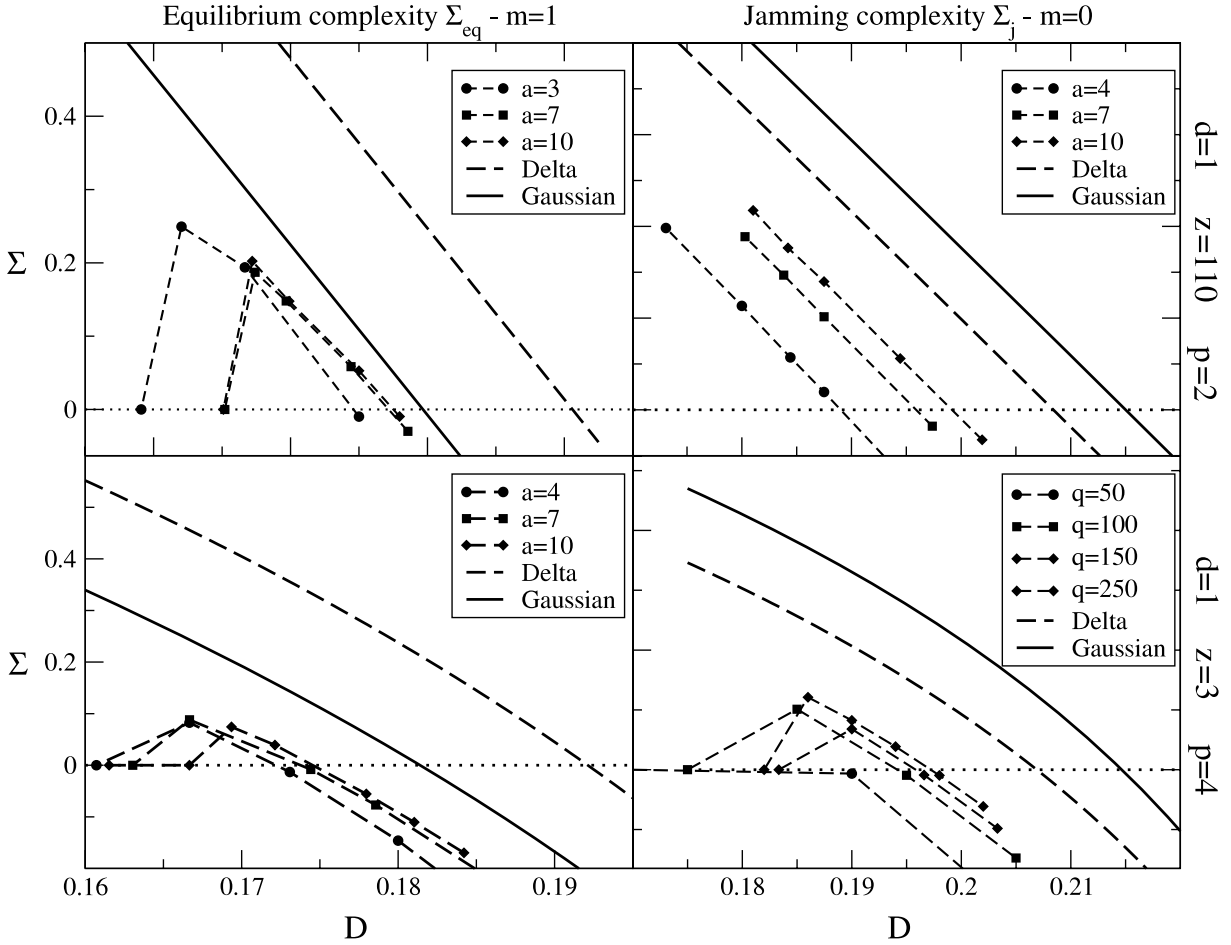
Figure 5. The complexity in some representative cases of discontinuous transitions at $d = 1$, computed with the numerical solution of the population dynamics algorithm with varying resolution of the discretization process, is compared to the Gaussian and delta approximations. Upper panels: Σ_{eq} (left) and Σ_j (right) for $p = 2$ and $z = 110$. In both cases we fixed the parameter $a = 4, 7, 10$ in equation (69) and changed q to vary the effective diameter $D_{\mathrm{eff}} = (1 + 2a)/(2q)$, which is reported on the horizontal axis. Lower panel: Σ_{eq} (left) and Σ_j (right) for $p = 4$ and $z = 3$. In the first case, we varied q at fixed a, while in the second we did the opposite.

sampled uniformly) and Σ_j (the complexity at $m = 0$ equal to $(1/N)$ times the logarithm of the total number of jammed states) for several representative cases at $d = 1$ where the transition is discontinuous. Generically we observe that the delta approximation performs better at $m = 0$, while the Gaussian approximation is more reliable at $m = 1$. Both approximations give an upper bound to the true complexity and therefore give values for D_{K} and D_{GCP} that are above the true ones. Moreover, both approximations miss the dynamical transition since by construction the fields are assumed to be localized.

Some results for $d = 2$ are reported in figure 6. Here the scaling for $q \to \infty$ becomes very difficult because the numerical solution is computationally demanding and we cannot go beyond $q = 20$ for moderate connectivities. We could perform a systematic

Figure 6. The complexity at $d = 2$, $p = 2$ and $z = 20$, computed with the numerical solution of the population dynamics algorithm with varying resolution of the discretization process, is compared to the Gaussian and delta approximations. Here we can only use moderate values of q, and because of the geometry of the discretization the effective diameter of the sphere, given by equation (70) and reported on the horizontal axis, cannot be varied smoothly. For instance, at $q = 11$ we could not find a point at positive complexity.

investigation only $p = 2$ and $z = 20$, which is unfortunately a case where the transition is continuous and the solution might be unstable towards further RSB in the glass phase. In this case, at $m = 1$ we correctly find a continuous transition at a value of D which is compatible with the result found from the stability analysis of section 4. At $m = 0$, we find good agreement with the results of the Gaussian and delta approximations. Note however that also at $m = 0$ the results could be unstable towards further RSB.

8.2. Phase diagram

In figure 7 we compare the transition lines obtained by the Gaussian and delta approximations with the numerical results, where available. We computed D_{K} and D_{GCP} by performing an extrapolation to $q \to \infty$ (which is simple since the corrections are found to be proportional to $1/q$) in some representative cases where the transition is continuous or discontinuous; the results are reported in figure 7. We observe that indeed the Gaussian and delta approximations give consistent results, which are also consistent with the exact numerical solution and provide upper bounds to the latter.

Whenever the RS instability $D_{\mathrm{RS}} < D_{\mathrm{K}}$, the transition is continuous. This happens generically for small z. On increasing z, the lines D_{RS} and D_{K} cross and the transition becomes discontinuous. The value z^* where this crossover happens depends weakly on the space dimension, but it depends strongly on p. Indeed we have $z^* \sim 100$ for $p = 2$, while $z^* \sim 20$ for $p = 3$ and (as we can infer from figure 4) the transition is always discontinuous for $p > 3$.
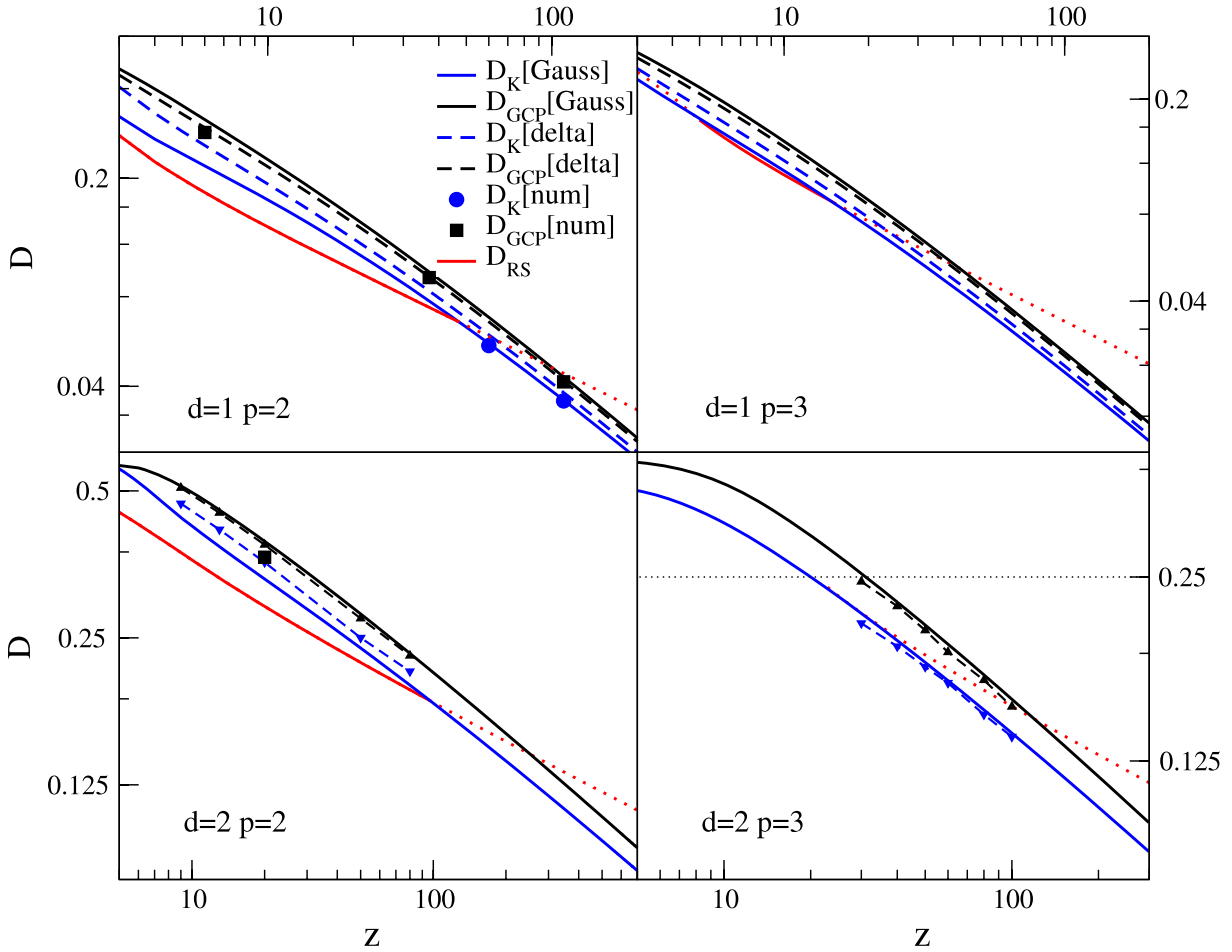
Figure 7. Phase diagrams for $p = 2, 3$ and $d = 1, 2$. We compare the results of the Gaussian and delta approximations with the numerical results obtained directly from a discretization of the cavity equations. In the lower right panel, the horizontal line indicates the value $D = 1/4$ above which the calculation of Z_3^0 is not valid, see equation (29).

9. Correlation function

9.1. Definition

As explained in section 3, in the glass phase the cavity equations have multiple solutions, each describing a different glass state. Within each state α we can define a correlation function $g_\alpha(x, y)$ as follows. For each box we have

$$
g_a^{(\alpha)}(x, y) = \frac{1}{p(p-1)} \left\langle \sum_{i \neq j}^{1,p} \delta(x - x_i)\delta(y - x_j) \right\rangle_{a,\alpha} = \frac{1}{p(p-1)}
$$

$$
\times \frac{\int \mathrm{d}x_1^a \cdots \mathrm{d}x_p^a \, \psi_{a,1}^{(\alpha)}(x_1^a) \cdots \psi_{a,p}^{(\alpha)}(x_p^a) \, \chi(x_1^a, \ldots, x_p^a) \sum_{i \neq j}^{1,p} \delta(x - x_i^a)\delta(y - x_j^a)}{\int \mathrm{d}x_1^a \cdots \mathrm{d}x_p^a \, \psi_{a,1}^{(\alpha)}(x_1^a) \cdots \psi_{a,p}^{(\alpha)}(x_p^a) \, \chi(x_1^a, \ldots, x_p^a)},
$$

$$(79)$$

since the fields $\psi_{a,i}^{(\alpha)}(x_i^a)$ describe the distribution of the variables adjacent to box a in the absence of the box itself. We now average this quantity over the boxes and over the states α with the weight Z_α^m. We get

$$
\begin{aligned}
g(x,y) &= \frac{p}{Nz} \sum_{a=1}^{Nz/p} \frac{1}{\sum_\alpha Z_\alpha^m} \sum_\alpha g_a^{(\alpha)}(x,y) Z_\alpha^m \\
&= \mathrm{e}^{-S_{\mathrm{box}}} \int \mathrm{d}\mathcal{P}[\psi_1] \cdots \mathrm{d}\mathcal{P}[\psi_p] \, Z_{\mathrm{box}}[\psi_1 \cdots \psi_p]^{m-1} \, \psi_1(x)\psi_2(y) \\
&\quad \times \int \left(\prod_{j=3}^p \psi_j(x_j) \, \mathrm{d}x_j \right) \chi(x,y,x_3,\ldots,x_p).
\end{aligned}
\tag{80}
$$

Note that in the RS case the above expression reduces to $g_p^0(x,y)$.

We expect that at $m=0$ (close packing), $g(x,y)$ develops a peak in $|x-y|=D$ describing contacts [27, 28]. The number of contacts is

$$
\zeta = (p-1) \int_{\mathrm{peak}} g(0,y) \, \mathrm{d}y.
\tag{81}
$$

The delta peak is also accompanied, in three-dimensional sphere packings, by a square root divergence, $g(r) \sim (r-D)^{-0.5}$ [27, 28], which we want to investigate here.

Note that in the delta approximation we just get

$$
g(x,y) = \frac{1}{Z_p^0} \int \mathrm{d}X_3 \cdots \mathrm{d}X_p \, \chi(x,y,X_3,\ldots,X_p) = g_p^0(x,y);
\tag{82}
$$

therefore all the structure of the correlation in the packings is lost in this approximation.

One can show, following [5], that in the Gaussian approximation, as $A \sim m$ for $m \to 0$, one gets a delta peak at $r=D$ in the jamming limit, with all particles being non-rattlers and $\zeta = 2d$. Therefore, this approximation is able to capture some of the peculiar structure of the correlation. On the other hand, the square root singularity is missed by the Gaussian approximation [5].

Unfortunately, it is very difficult to study the contact peak in the numerical solution of the cavity equation, because the discretization makes it hard to define a proper notion of contacts and separate the delta peak contribution from the background. Therefore, in the following we focus on the square root singularity which is also a non-trivial and somehow unexpected feature of pair correlations at jamming [27, 28].

Numerical results are presented in figure 8 for the $g(r)$ in one dimension, and two representative values of z and p where the transition is continuous or discontinuous. In both cases, the divergence is compatible with a square root singularity $(r-D)^{-0.5}$ in a range of $r-D$, but at smaller $r-D$ the $g(r)$ seems to diverge as $(r-D)^{-\gamma}$ with an exponent $\gamma > 0.5$. However, in this region the square root divergence is probably mixed with the contact delta peak, because of the discretization. A detailed analysis of this mixing was not possible because the values of q we could reach were still too small. Since this investigation is computationally very demanding, we could not perform a systematic study of the value of the exponent as a function of p and z, nor investigate the more interesting case $d=2$, which is very difficult because our discretization does not preserve the spherical symmetry around the central particle. We leave a more systematic numerical analysis for future work.
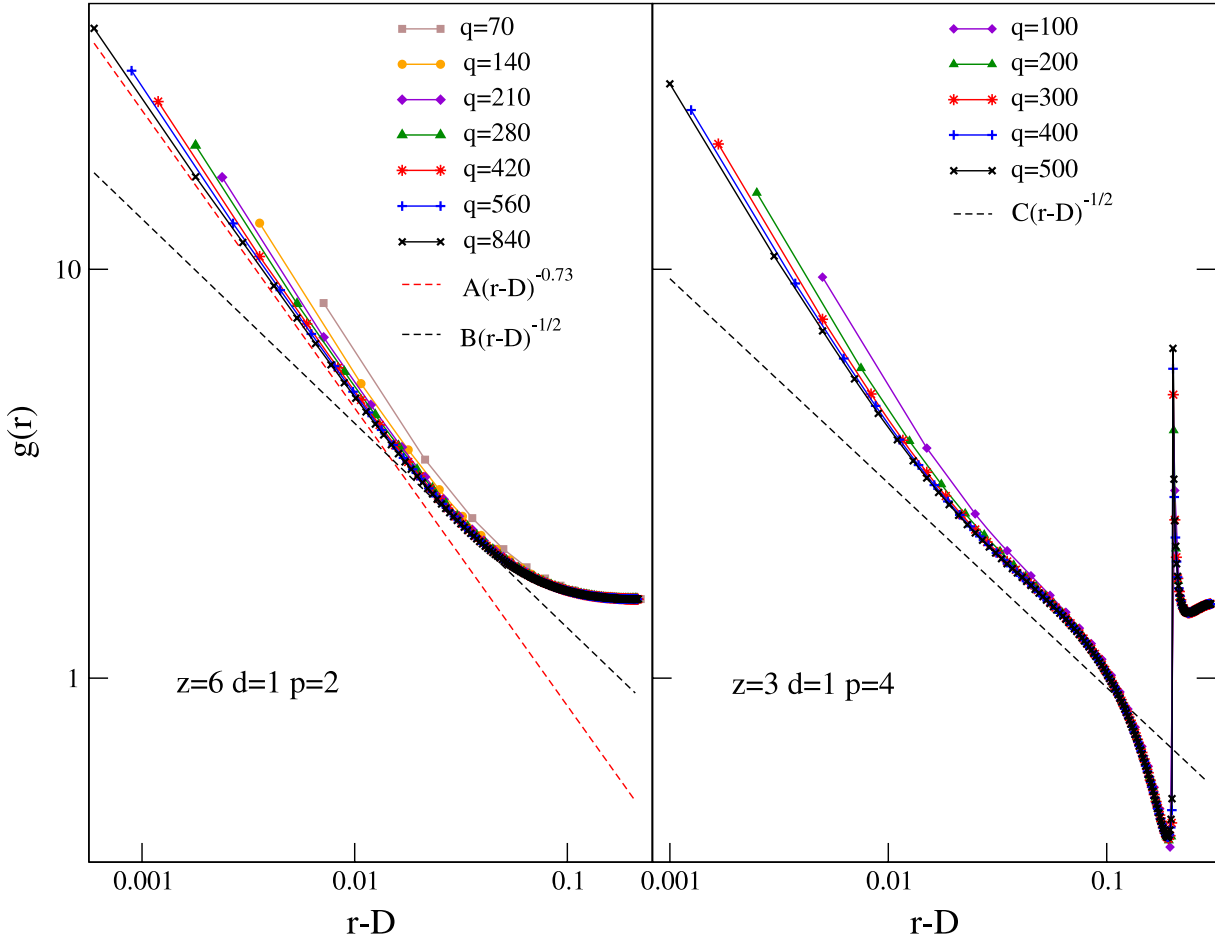
Figure 8. Pair correlation function $g(r)$ at $d = 1$, $m = 0$ (jamming) and $D \sim D_{\mathrm{GCP}}$ (in practice, the closest value to D_{GCP} compatible with the discretization). Left: $p = 2$, $z = 6$; note that in this case the system undergoes a continuous transition and these results might be unstable towards further RSB. Right: $p = 4$, $z = 3$; here the transition is discontinuous. Note that for $p = 4$ we observe an additional singularity at $r = 2D$ [27].

9.2. Argument for the square root singularity

We now present an analytical argument to relate the shape of the cavity fields to the square root singularity. We focus on $m = 0$, and we study the small $r - D$ behavior of $g(r)$ as follows. We define the quantity

$$\Psi(z) = \int \left(\prod_{j=1}^{p} \psi_j(x_j) \, \mathrm{d}x_j \right) \frac{\chi(x_1, \ldots, x_p)}{\chi(x_1, x_2)} \delta(x_1 - x_2 - z). \tag{83}$$

Note that $z = x - y \in [-1, 1]^d$ but using periodicity one can restrict to $z \in [-1/2, 1/2]^d$ with periodic boundary conditions. The probability distribution of ψ induces

a distribution $\mathcal{P}[\Psi]$ on Ψ. Then we have

$$g(z) = \int \mathrm{d}x\,\mathrm{d}y\,g(x,y)\delta(x-y-z) = \mathrm{e}^{-S_{\mathrm{box}}} \int \mathrm{d}\mathcal{P}[\Psi] \frac{\Psi(z)\chi(z)}{\int \mathrm{d}z\,\Psi(z)\chi(z)} \theta\left[\int \mathrm{d}z\,\Psi(z)\chi(z)\right],$$
(84)

where the term $\mathrm{e}^{-S_{\mathrm{box}}}$ ensures the normalization $\int \mathrm{d}z\,g(z) = 1$.

In the following we restrict for simplicity to $d = 1$. Note that by translational invariance the field Ψ is centered around a random uniformly distributed position z_0, while its shape is encoded by a non-trivial distribution. Now assume that with a certain finite probability with respect to the shape distribution, one has the following.

- $\Psi(z)$ vanishes at some finite distance from the center given by $z_\pm = z_0 \pm \delta z_0$. The quantities $z_\pm$ are then also random and uniformly distributed in $[-1/2, 1/2]$.

- The shape of $\Psi(z)$ around the point where it vanishes is of the form

$$\Psi(z) \sim \mathrm{e}^{-A/(|z-z_\pm|^\alpha)}.$$
(85)

- $|z_+ - z_-| < 2D$, and $z_+ > D$ (the additional symmetric contribution coming from z_- gives a factor 2 and will be neglected as well as all proportionality constants).

Then the function $\chi(z)\Psi(z)$ vanishes everywhere except in $[D, z_+]$, where it is given by $\exp[-A/(z_+ - z)^\alpha]$. The average over $\mathcal{P}[\Psi]$, for what concerns this contribution, is translated onto an average over z_+ and equation (84) becomes

$$g(z) \sim \int \mathrm{d}z_+ \frac{\mathrm{e}^{-A/(z_+-z)^\alpha}\theta(D \le z \le z_+)}{\int_D^{z_+}\mathrm{d}z\,\mathrm{e}^{-A/(z_+-z)^\alpha}}\theta[z_+ \ge D] = \int_z^C \mathrm{d}z_+ \frac{\mathrm{e}^{-A/(z_+-z)^\alpha}}{\int_D^{z_+}\mathrm{d}z\,\mathrm{e}^{-A/(z_+-z)^\alpha}},$$
(86)

where C is a suitable cutoff that comes from the fact that if z_+ is too much larger than D the approximation (85) will break down. We will show that this cutoff does not matter as the main contribution for $z \to D$ comes from z_+ close to D.

To simplify notations, we introduce $\lambda = (z - D)/D$ and $\varepsilon = (z_+ - D)/D$. Also we define $a = A/D^\alpha$ and $c = (C - D)/D$. With these notations we get

$$g(\lambda) \propto \int_\lambda^c \mathrm{d}\varepsilon \frac{\mathrm{e}^{-a/(\varepsilon-\lambda)^\alpha}}{\int_0^\varepsilon \mathrm{d}\lambda\,\mathrm{e}^{-a/(\varepsilon-\lambda)^\alpha}}.$$
(87)

The integral in the denominator is dominated by the small λ behavior, that gives

$$\int_0^\varepsilon \mathrm{d}\lambda\,\mathrm{e}^{-a/(\varepsilon-\lambda)^\alpha} \sim \int_0^\varepsilon \mathrm{d}\lambda\,\mathrm{e}^{-(a/\varepsilon^\alpha)(1+\alpha(\lambda/\varepsilon))} = \mathrm{e}^{-a/\varepsilon^\alpha}\frac{\varepsilon^{\alpha+1}}{a\alpha},$$
(88)

and

$$g(\lambda) \propto \int_\lambda^c \mathrm{d}\varepsilon\,\varepsilon^{-(\alpha+1)}\mathrm{e}^{a(1/\varepsilon^\alpha-(1/(\varepsilon-\lambda)^\alpha))}.$$
(89)

We want now to evaluate the integral by a saddle point for $\lambda \to 0$. We assume (and will check self-consistently) that the saddle point value $\varepsilon^* \gg \lambda$. Then we can expand for $\lambda/\varepsilon \ll 1$ and

$$g(\lambda) \propto \int_\lambda^c \mathrm{d}\varepsilon\,\mathrm{e}^{-(\alpha+1)\log\varepsilon - a\alpha\lambda\varepsilon^{-(\alpha+1)}}.$$
(90)

The maximum of the above expression is found at $\varepsilon^* = (a\alpha\lambda)^{1/(\alpha+1)} \gg \lambda$ for small λ as initially assumed. Substituting this in the expression above one obtains $g(\lambda) \propto 1/\lambda$. To get the correct result we need to compute also the quadratic corrections around the saddle point. Including these, we finally obtain

$$g(\lambda) \propto \lambda^{-\alpha/(1+\alpha)} \propto (r - D)^{-\alpha/(1+\alpha)}, \qquad (91)$$

i.e. a power-law divergence for $z \to D$ with exponent $\in [0, 1]$, which is consistent with the observed exponents in figure 8. Note that a square root singularity is obtained for $\alpha = 1$, namely a simple exponential singularity of the cavity fields. We checked in our numerical results that indeed the form of the fields is compatible with the ansatz (85).

Note that this same argument can be carried out at finite m, but in this case we get that $g(\lambda)$ is independent of λ for small λ. A more complete analysis should show that at finite m, $g(\lambda)$ is a power law for $\lambda \gg O(m^\nu)$ with some exponent ν, and it crosses over to a finite value for $\lambda \ll O(m^\nu)$.

10. Discussion on finite dimensional hard spheres

One way to recover the normal hard sphere model from our model is to set $p = 2$ and $z = N - 1$. However, this limit cannot be investigated within the cavity formalism which is based on taking first the limit $N \to \infty$ at finite z. Here the limits $N \to \infty$ and $z \to \infty$ do not commute, and if we first send $N \to \infty$ and then $z \to \infty$ we do not recover the hard sphere models (a similar behavior is found for the Bethe lattice spin glass [23]).

Therefore we want here to find a suitable limit that we can take after $N \to \infty$ to recover the hard sphere model. As we discussed in section 1, one possibility if to set formally $z = 1$ and identify p with the number of particles, therefore taking $p \gg 1$. Of course, for $z \leq 2$ and finite p the model does not have any phase transition (it becomes a one-dimensional model for $z = 2$). Therefore, we have to send $p \to \infty$ before z becomes smaller than two.

As a first check, we note that in this limit the RS entropy

$$S^{\mathrm{RS}} = \frac{z}{p} \log Z_p^0 \to S_{\mathrm{liq}}(\varphi), \qquad (92)$$

where $S_{\mathrm{liq}}(\varphi)$ is the entropy of d-dimensional hard spheres in the thermodynamic limit at fixed packing fraction φ. Actually, there is a problem with the latter identification, since Z_p^0 does not contain a factor $p!$ which should take into account indistinguishability of the particles. This is indeed to be expected, since we took a formal limit $z \to 1$, but at any finite $z > 1$ the particles are connected to several boxes which makes them distinguishable. We therefore recover the finite dimensional result for a system of distinguishable particles.

Next, we can look at the stability of the RS solution according to equation (20). To compare with standard hard spheres it is crucial to observe that here the box side is one while D becomes very small for $p \to \infty$, in such a way that the packing fraction $\varphi = p V_d(D/2) = p V_d(1/2) D^d$ is finite. For $p \to \infty$ first and $z \to 1$ after, we have $g_p^0(x) \to g_{\mathrm{liq}}(x)$, however x is expressed in units of the box length. If we introduce as usual the distance r measured in units of the sphere diameter, $r = x/D$, we have (for $k \neq 0$)

$$g_p^0(k) = \int \mathrm{d}x \, \mathrm{e}^{\mathrm{i}kx} g_p^0(x) = D^d \int \mathrm{d}r \, \mathrm{e}^{\mathrm{i}kDr} g_{\mathrm{liq}}(r) = D^d S(kD), \qquad (93)$$

where $S(kD)$ is the structure factor, and the stability condition becomes

$$\sqrt{(p-1)(z-1)}D^d|S(kD)| = \sqrt{(p-1)(z-1)}\frac{\varphi}{pV_d(1/2)}|S(kD)| \le 1, \quad (94)$$

which is always verified for $p \to \infty$ since φ and $S(kD)$ are both of order one. This is indeed consistent with our investigations of the model at finite p that showed that the transition is always discontinuous at $p > 4$. We conclude that one cannot observe a continuous transition in the normal hard spheres model. This conclusion is consistent with those of Biroli and Bouchaud [29] who showed that indeed replicated liquid theory in finite dimensions does not allow for a continuous RSB transition.

We also note that starting from equations (43) and (42) and taking first $p \to \infty$ (with $\varphi = pV_d(D)/2^d$ and $(p-1)g_p^0(r) = pg_{\text{liq}}(r)$) and then $z \to 1$ we recover equation (74) of [5], which is the starting point of the Gaussian small cage replica treatment in finite dimensions, provided we identify again $\lim_{p\to\infty}(1/p)\log Z_p^0 = S_{\text{liq}}(\varphi)$, neglecting the problem with the missing $p!$. Apart from this caveat, this is a nice alternative derivation of the approximation of [5], which is not based on the replica method.

Finally, one could try to take the same formal limit in equation (52) to obtain an alternative approximate expression for $S(m)$ in finite dimensions. Using the relation $Z_p^0/Z_{p-1}^0 = \langle v \rangle$, where v is the void space of $p - 1$ particles, we obtain for $z \to 1$ (after $p \to \infty$)

$$S(m) = \log\frac{\langle v^m \rangle}{\langle v \rangle} + \frac{1}{p}\log Z_p^0. \quad (95)$$

Note however that the void space $v \propto p$, therefore we must rearrange terms as

$$S(m) = \log\frac{\langle (v/p)^m \rangle}{\langle (v/p) \rangle} + m\log p + \frac{1}{p}\log(Z_p^0/p^p). \quad (96)$$

The term $m\log p$ can be dropped since it gives an additive constant to the internal entropy, and the resulting expression has a well defined $p \to \infty$ limit, assuming here that $\lim_{p\to\infty}(1/p)\log(Z_p^0/p!) = S_{\text{liq}}(\varphi)$ (which is, however, inconsistent with the previous discussion, for reasons that we do not understand at present). This expression can in principle be directly computed, even if it is very hard to sample the distribution $P(v)$ of void space because at high density $v = 0$ for most configurations [30].

11. Conclusions

In this paper, we have studied a mean-field hard sphere model introduced in [12]. The model is similar to a standard hard sphere model, however each sphere interacts only with a finite and preassigned number of neighbors. The network of interactions is given by a random graph, such that the model belongs to the mean-field class and is therefore, in principle, exactly solvable via the cavity method. We therefore derived the cavity equations for the model and we presented both analytical approximations to their solution and an 'exact' numerical solution based on a discretization of the space.

We have shown that the analytical approximations give quite reliable results for the phase diagram and the complexity. In particular, for large enough z and/or p, the transition belongs to the random first order class. Therefore, as suggested in [12], the

model displays an ideal glass (Kauzmann) transition to a glass phase. Following the glass phase upon increasing pressure, one gets to a point where the pressure diverges, similarly to standard hard spheres close to the so-called J-point. Given that the model has an exponential number of metastable states, one obtains a set of J-points spanning a finite range in density. Overall, the phenomenology of the model in this regime is very close to that expected for finite dimensional hard spheres based on mean-field approximations, see [5] and figure 1. We found, in particular, that the Gaussian approximation is very good for the Kauzmann transition but tends to overestimate the close packing. This is consistent with what happens for three-dimensional hard spheres where the Gaussian approximation gives $\varphi_{\mathrm{K}} \sim 0.62$, which is consistent with numerical estimates, and $\varphi_{\mathrm{GCP}} \sim 0.68$, while numerical simulations suggest a somewhat smaller value [5]. On the contrary, the delta approximation is very good for close packing but tends to overestimate the Kauzmann point. We proposed a formula for the complexity that is based on the delta approximation and can be computed numerically for three-dimensional hard spheres. It would be very interesting to do this computation and compare the result with the Gaussian approximation in that case.

We also found a somehow unexpected result, that the transition is continuous at small z and p. In particular, for the values of $p = 2$ and $z = 100$ that have been used in [12], the transition should be very weakly first order. The physics in the presence of a second order transition could be very different. For instance, in the case of the Sherrington–Kirkpatrick model, the intensive ground state energy can be found easily; this would correspond to a unique J-point density. However, the details of this depend on the model, and in particular on the shape of the complexity function, so we cannot give any conclusive statement. It would be interesting to investigate better this point by repeating the numerical simulations of [12] both in a region where the transition should be strongly second order (e.g. at $p = 2$ and small z) and in a region where it should be strongly 'random first order' (e.g. for $p = 4$ and small z).

Finally, we partially investigated the structure of the configurations at jamming. We computed the correlation function of the model and showed that it displays a power-law singularity close to contact, at least for $d = 1$. We also gave an analytical argument to explain the mathematical origin of the singularity. Extending this study to higher dimension could give insight into the physics that is responsible for this divergence and hopefully connect it to isostaticity and the presence of soft modes in the spectrum, as suggested in [14, 15]. Additional numerical simulations could be extremely useful also in this respect.

Acknowledgments

References

[1] Stoessel J P and Wolynes P G, 1984 *J. Chem. Phys.* **80** 4502
[2] Singh Y, Stoessel J P and Wolynes P G, 1985 *Phys. Rev. Lett.* **54** 1059
[3] Speedy R J, 1998 *Mol. Phys.* **95** 169
[4] Cardenas M, Franz S and Parisi G, 1998 *J. Phys. A: Math. Gen.* **31** L163
[5] Parisi G and Zamponi F, 2010 *Rev. Mod. Phys.* **82** 789
[6] Stillinger F H and Weber T A, 1982 *Phys. Rev.* A **25** 978

[7] Lubachevsky B D and Stillinger F H, 1990 *J. Stat. Phys.* **60** 561
[8] Krzakala F and Kurchan J, 2007 *Phys. Rev.* E **76** 021122
[9] Monasson R, 1995 *Phys. Rev. Lett.* **75** 2847
[10] Mézard M and Parisi G, 1999 *J. Chem. Phys.* **111** 1076
[11] Castellani T and Cavagna A, 2005 *J. Stat. Mech.* P05012
[12] Mari R, Krzakala F and Kurchan J, 2009 *Phys. Rev. Lett.* **103** 025701
[13] O'Hern C S, Silbert L E, Liu A J and Nagel S R, 2003 *Phys. Rev.* E **68** 011306
[14] Wyart M, 2005 *Ann. Phys.* **30** 1 [arXiv:cond-mat/0512155]
[15] Wyart M, Nagel S and Witten T, 2005 *Europhys. Lett.* **72** 486
[16] Mézard M, Parisi G and Virasoro M A, 1987 *Spin Glass Theory and Beyond* (Singapore: World Scientific)
[17] Mézard M and Montanari A, 2009 *Information, Physics and Computation* (Oxford: Oxford University Press)
[18] Van Hecke M, 2010 *J. Phys.: Condens. Matter* **22** 033101
[19] Liu A, Nagel S, Van Saarloos W and Wyart M, 2011 *Dynamical Heterogeneities and Glasses* ed L Berthier, G Biroli, J-P Bouchaud, L Cipelletti and W van Saarloos (Oxford: Oxford University Press) arXiv:1006.2365
[20] Torquato S and Stillinger F H, 2010 *Rev. Mod. Phys.* **82** 2633
[21] Parisi G, 2007 *Complex Systems* ed J-P Bouchaud, M Mézard and J Dalibard (Les Houches: Elsevier) arXiv:0706.0094
[22] Hansen J-P and McDonald I R, 1986 *Theory of Simple Liquids* (London: Academic)
[23] Mézard M and Parisi G, 2001 *Eur. Phys. J.* B **20** 217
[24] Rintoul M D and Torquato S, 1995 *Phys. Rev.* E **52** 2635
[25] Zdeborová L and Krzakala F, 2007 *Phys. Rev.* E **76** 031131
[26] Mézard M and Montanari A, 2006 *J. Stat. Phys.* **124** 1317
[27] Silbert L E, Liu A J and Nagel S R, 2006 *Phys. Rev.* E **73** 041304
[28] Donev A, Torquato S and Stillinger F H, 2005 *Phys. Rev.* E **71** 011105
[29] Biroli G and Bouchaud J, 2009 arXiv:0912.2542
[30] Sastry S, Truskett T, Debenedetti P, Torquato S and Stillinger F, 1998 *Mol. Phys.* **95** 289